

this document downloaded from

vulcanhammer.info

the website about
Vulcan Iron Works
Inc. and the pile
driving equipment it
manufactured

Visit our companion site
<http://www.vulcanhammer.org>

Terms and Conditions of Use:

All of the information, data and computer software ("information") presented on this web site is for general information only. While every effort will be made to insure its accuracy, this information should not be used or relied on for any specific application without independent, competent professional examination and verification of its accuracy, suitability and applicability by a licensed professional. Anyone making use of this information does so at his or her own risk and assumes any and all liability resulting from such use. The entire risk as to quality or usability of the information contained within is with the reader. In no event will this web page or webmaster be held liable, nor does this web page or its webmaster provide insurance against liability, for any damages including lost profits, lost savings or any other incidental or consequential damages arising from the use or inability to use the information contained within.

This site is not an official site of Prentice-Hall, Pile Buck, or Vulcan Foundation Equipment. All references to sources of software, equipment, parts, service or repairs do not constitute an endorsement.

**Modelling of Penetration Resistance and Static
Capacity of Piles Driven by Vibration at the
Pioneer Freezer Site, Syracuse, NY, and Laboratory Model Tests**

a Report to the Deep Foundations Institute

by Michael W. O'Neill and Cumaraswamy Vipulanandan,
Co-Principal Investigators,

and Reda Moulai-Khatir,
Graduate Research Assistant

Department of Civil and Environmental Engineering
University of Houston

October 1, 1991

Table of Contents

Topic	Page
Introduction	1
Background	1
Scope	3
Field Testing Conditions	5
Laboratory Testing Arrangement for Model Piles	8
Static Capacity Evaluation	16
Test Results	17
Wave Equation Analysis	18
General	18
Formulation of the Wave Equation for Cyclic Force Analysis (Mod. 1)	21
Formulation of the Wave Equation for Analysis with Vibrator (Mod. 2)	24
Optimization of Parameters	30
First Stage Optimization	30
Second Stage Optimization	33
Sensitivity Study	34
Conclusions	34
Acknowledgments	36
References	36
Appendix A	37
Appendix B	45
Appendix C	47
Appendix D	62
Appendix E	70

**Modelling of Penetration Resistance and Static
Capacity of Piles Driven by Vibration at the
Pioneer Freezer Site, Syracuse, NY, and Laboratory Model Test**

INTRODUCTION

Background

Vibratory driving is a technique used for driving piles into the ground by imparting to the pile a small longitudinal vibratory motion of a predetermined frequency and displacement amplitude from a driving unit. The vibrations serve to reduce the ground resistance, allowing penetration under the action of a relatively small surcharge, or "biased" load, also provided by the driving unit, or "hammer." A schematic of a typical vibratory hammer-pile-soil system is shown in Fig. 1. Vibratory driving is especially effective in cohesionless soils and is favored over impact driving from the perspective of rapid and silent operation. However, the use of vibratory drivers has been hampered by the inability of inspection agencies to verify the bearing capacity of installed piles in the manner afforded by wave equation analysis of impact-driven piles. The current accepted practice requires restriking the vibro-driven piles with an impact hammer to verify the capacity by means of wave equation analysis or by direct dynamic monitoring. This operation increases the time required to install piles with the use of vibratory drivers and makes the process less attractive economically than it would be if some straightforward procedure were available to evaluate capacity from pile and hammer properties and simple parameters, such as rate of penetration at full penetration, that can be observed by an on-site inspector. The study reported herein aims to extend the one-dimensional wave equation approach to predict the capacity of several full-scale and model piles to demonstrate that an appropriately modified wave equation program can be used in certain cases. Further research is necessary to generalize the results of this study.

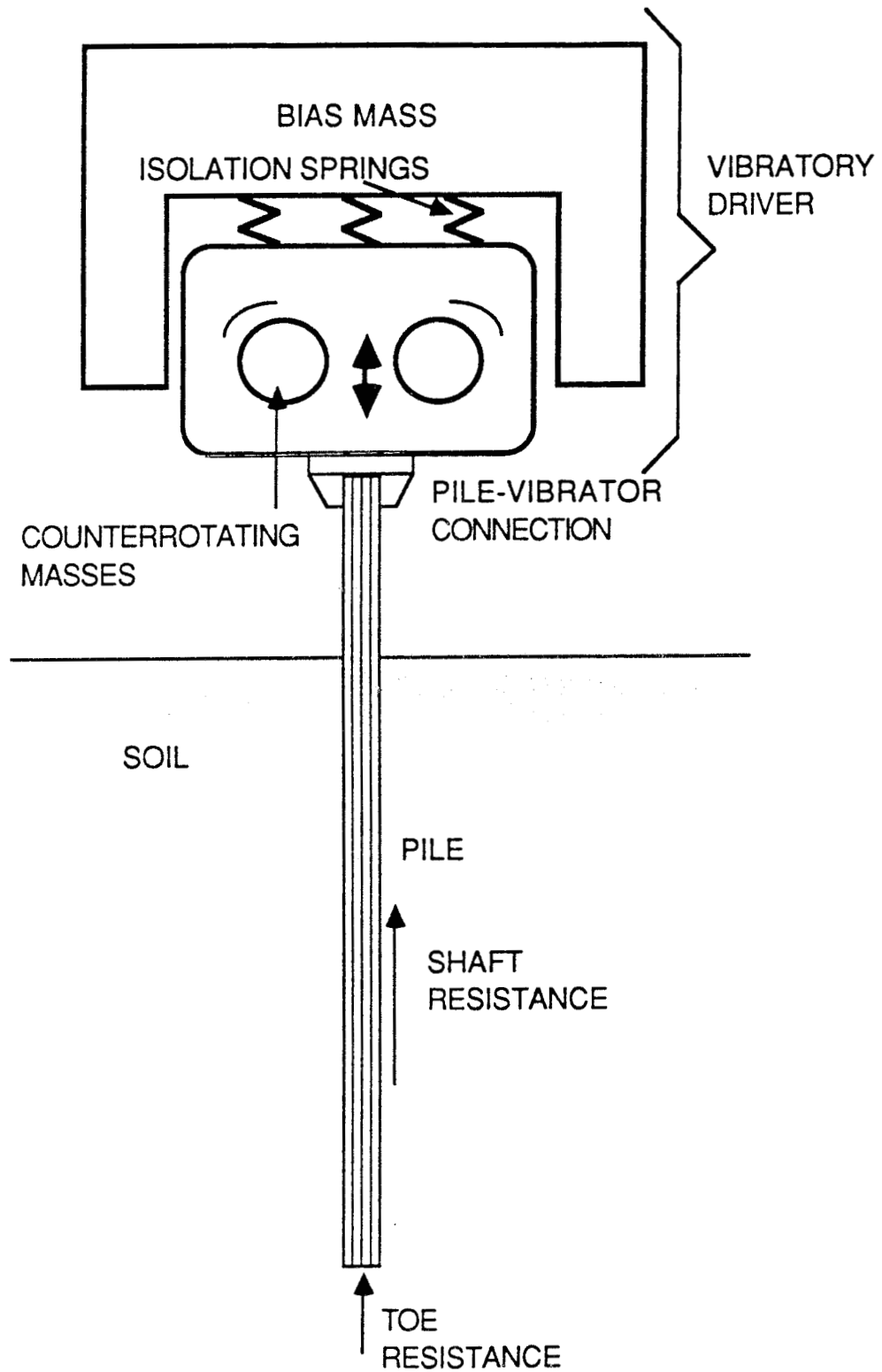


Fig. 1. Schematic of Typical Vibro-Driver and Pile

In mid-1985, the Deep Foundations Institute (DFI) issued a request for proposals to a wide range of organizations for assistance in developing analytical techniques for predicting the capacity of bearing piles installed with vibratory hammers. The original proposal was quite extensive in order to support fully the data needs to develop the prediction techniques. Unfortunately, after a year of effort by a DFI special subcommittee, the logistics and funding could not be developed for the major effort originally envisioned. At the DFI 1986 fall meeting in Houston, Texas, the decision was made to immediately proceed with a greatly reduced program so that access could be gained to an available test site at Hunter's Point in San Francisco, California, where the Federal Highway Administration and the US Army Corps of Engineers had just completed an extensive pile testing program. About three years later and also as a consequence of the DFI request, a work plan for field testing and data acquisition at another site, the Pioneer Freezer Plant in Syracuse, New York, was developed. At both test sites, work plans for data acquisition were supervised and executed by the Soil and Rock Instrumentation Division (SRI) of Goldberg-Zoino & Associates, Inc. (GZA) and DFI (4, 5).

In July, 1989 the opportunity to obtain the above data for analytical purposes was presented to the University of Houston (UH) by Mr. William Loftus, representing DFI. Michael O'Neill of UH visited the Pioneer Freezer Site during that month, while static loading tests were proceeding. During the site visit geotechnical information about the site was acquired. During the fall meeting of DFI in October, 1989, in Baltimore, Maryland, DFI agreed to transmit the data to the University of Houston for analysis. UH agreed to work with the data at no cost on a time-available basis. This report summarizes the analyses that were possible to make with the data acquired.

Scope

The scope of UH's activities included the following:

1. Convert 4 and 7-track data tapes provided by GZA for both test sites to floppy disks for further analysis on microcomputers at UH. Assistance was given by USAE Waterways Experiment Station in reading and converting the Hunter's Point data tapes, which were not compatible with tape reader/recorders at UH.

2. Reduce the digitized data to useful engineering units by applying appropriate calibration constants and correlating various sequences of data with known events (driving, stopping for splicing, GZA data for rate of penetration, etc.).

3. Acquire from hammer manufacturers the necessary mechanical data to model the hammers used in the tests.

4. Evaluate the data in a preliminary manner to determine if further analysis was warranted. At this step it was concluded that the data from the Hunter's Point Site would require further modification, which UH was not prepared or qualified to make. The data from the Pioneer Freezer Site were observed to be reasonable without further modification.

5. Develop a computer program using the wave equation model to simulate the driving of the test piles. This wave equation model included a special model for the pile-driving hammer and an energy dissipator between the hammer and the pile head.

6. Conduct model tests of a closed-ended steel pipe pile and a steel H-pile in saturated, fine sand to assess whether model testing can be used to evaluate the necessary parameters for full-scale installation.

7. Using the Smith model to represent the soil, model the driving and static capacity of closed-end steel pipe piles and H piles at the Pioneer Freezer Site and the closed-end steel pipe and H model piles using the wave equation program developed for the project. Specifically, using measured pile-head force-time data as input, model the rate of

penetration and pile-head velocity-time history by systematic variation of the Smith parameters, total static capacity and the ratio of toe to total static resistance to infer optimum values for these parameters. Compare the optimized Smith parameters for the model pile with those for the full-sized pipe piles at the Pioneer Freezer Site.

8. Analyze the pile-soil-hammer system with the wave equation program using the optimized Smith parameters in order to evaluate the necessary mechanical energy dissipation features of the hammer and its connection to the pile.

9. Report the results of this effort to DFI (this document).

FIELD TESTING CONDITIONS

GZA's work plan was aimed at the collection of data related to the readily measurable characteristics of piles installed with vibratory pile hammers. To accomplish this goal, pile testing programs were performed at Hunter's Point in San Francisco, California, and the Pioneer Freezer Site in Syracuse, New York. The raw data collected from Hunter's point were not used because of problems encountered in reducing them into usable engineering data. The data from the Pioneer Freezer Site were found to be usable. Geotechnical conditions at that site are detailed in Appendix A.

The installation of several test piles at this site was performed from June 28 to July 5, 1989. Test piles TP1 and TP4 were vibrated and subjected to static loading tests. During installation pile-head force and velocity time histories were monitored with the Pile Dynamics Analyzer (PDA), and rates of penetration were recorded by video camera. The pile instrumentation scheme was set to allow for continuous recording of the pile-head dynamic force and acceleration. This was accomplished with two surface-mounted piezo-electric accelerometers and a full bridge strain transducer. The continuous accelerations and

force signals were recorded on a Vetter Model B 4-track FM tape recorder with calibration gain settings of 2.5 volts full scale. The fourth channel was used for voice input.

Test piles denoted TP2, TP3, TP5 and TP7 were impact-driven. Production piles 559, 619, 691, 754 and 825 were subsequently vibrodriven, with pile-head instrumentation similar to that for TP1 and TP4, and dynamically tested using an impact hammer, in which GZA determined static capacity from the PDA. Of interest are the vibrated test and production piles. Piles TP1 and the remaining production piles were all closed-end steel pipe piles. Pile TP4 was a steel H-pile. The test piles and production piles were vibro-driven to practical refusal, although the terminal penetration rate varied considerably.

To assess the wave equation computer program, Piles TP1, TP4 and 559 were selected for detailed analysis. Examination of the data indicated that the data for these piles were of the highest quality from among all of the test piles, although the data record that constitutes the end of driving of TP4 was lost. Some high-quality data were recovered at mid-depth for TP4, however. TP1 was a steel pipe pile, spiral welded, closed-end, with a 0.75-in. flat plate welded onto the toe, an outside diameter of 12 in., a wall thickness of 0.219 in. and a length of approximately 90 ft. The cross-sectional area of the steel was 8.11 in². TP1 was vibrated into position with an H-section welded to the head to provide a gripping surface for the vibrator to a penetration of 86 ft. The vibro-hammer used was an ICE 416 attached to the H-section by means of hydraulic clamps. A detail of that connection is shown in Fig. 2. The mechanical characteristics of the ICE 416 vibro-hammer are given in Appendix B.

Pile 559 was a closed-ended pipe pile with similar properties to those of TP1. The ICE 416 vibro-hammer was used to drive Pile 559 to practical refusal to a depth of 83 ft. Test pile TP4 was an HP 10X49 steel H pile approximately 90 ft long and was driven with

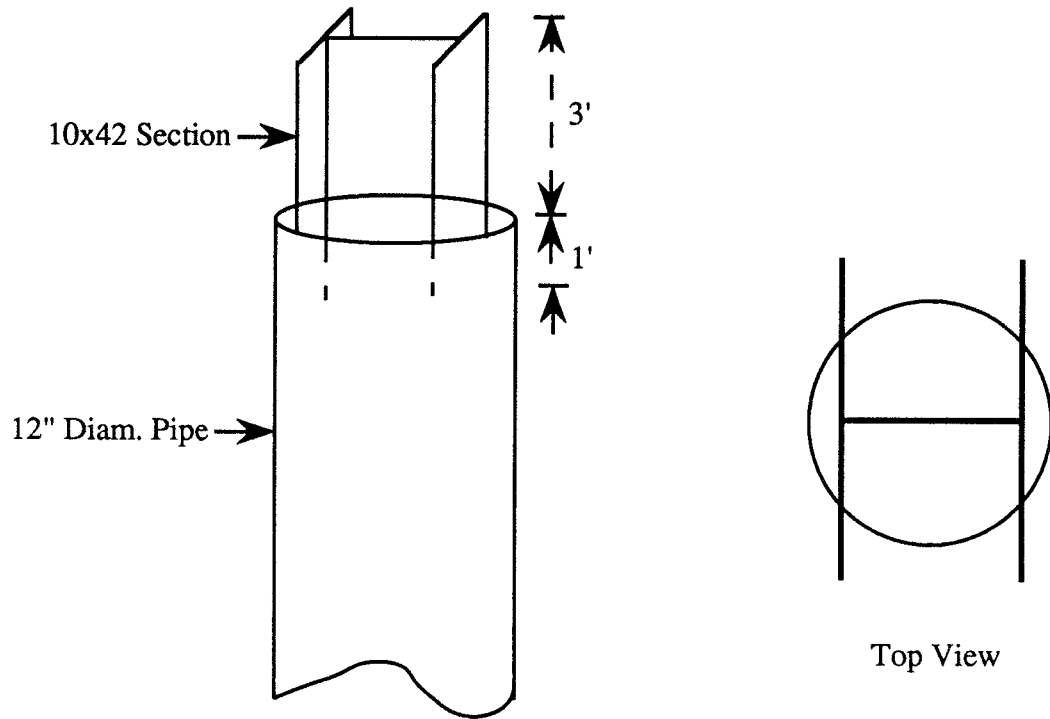


Fig. 2. Pile-Vibrator Connection Detail, Pioneer Freezer Site

the ICE 416 vibro-hammer to a penetration of about 80 ft. However, dynamic data could not be found on the data tapes beyond a penetration of about half of this value.

Rates of penetration were also recorded in the field using video cameras and are shown partially in Figs. 3 - 5 and in Appendix C in totality in tabular form.

It is noted that the test piles at the Pioneer Freezer Site were long and flexible and therefore required an analysis model that includes pile flexibility.

LABORATORY TESTING ARRANGEMENT FOR MODEL PILES

Two model pile tests were conducted in the UH geotechnical laboratory to investigate whether Smith soil parameters inferred from such tests can be applied to the field conditions at the Pioneer Freezer Site. An instrumented, closed-ended steel pile (per the pipe piles used at the Pioneer Freezer Site) approximately 95 in. long and 4.00 in. in diameter, was driven with a vibrator 78 in. into a pressurized sand column 30 in. in diameter, contained within a confining chamber located at the University of Houston. The test pile was made of cold drawn steel tubing and had a wall thickness of 0.188 in. Pile instrumentation included a strain gauge bridge and two piezoelectric accelerometers at the head of pile. This instrumentation and data recording systems were similar to those used during the vibratory installation of the test and production piles at the Pioneer Freezer Site. Additional instrumentation consisted of video camera monitors to record rates of penetration.

A similar test was conducted on a model steel H-pile (per Pile TP4), which was square in cross section, with a flange width and section depth of 3.00 in. and with flange and web thicknesses of 0.125 in.

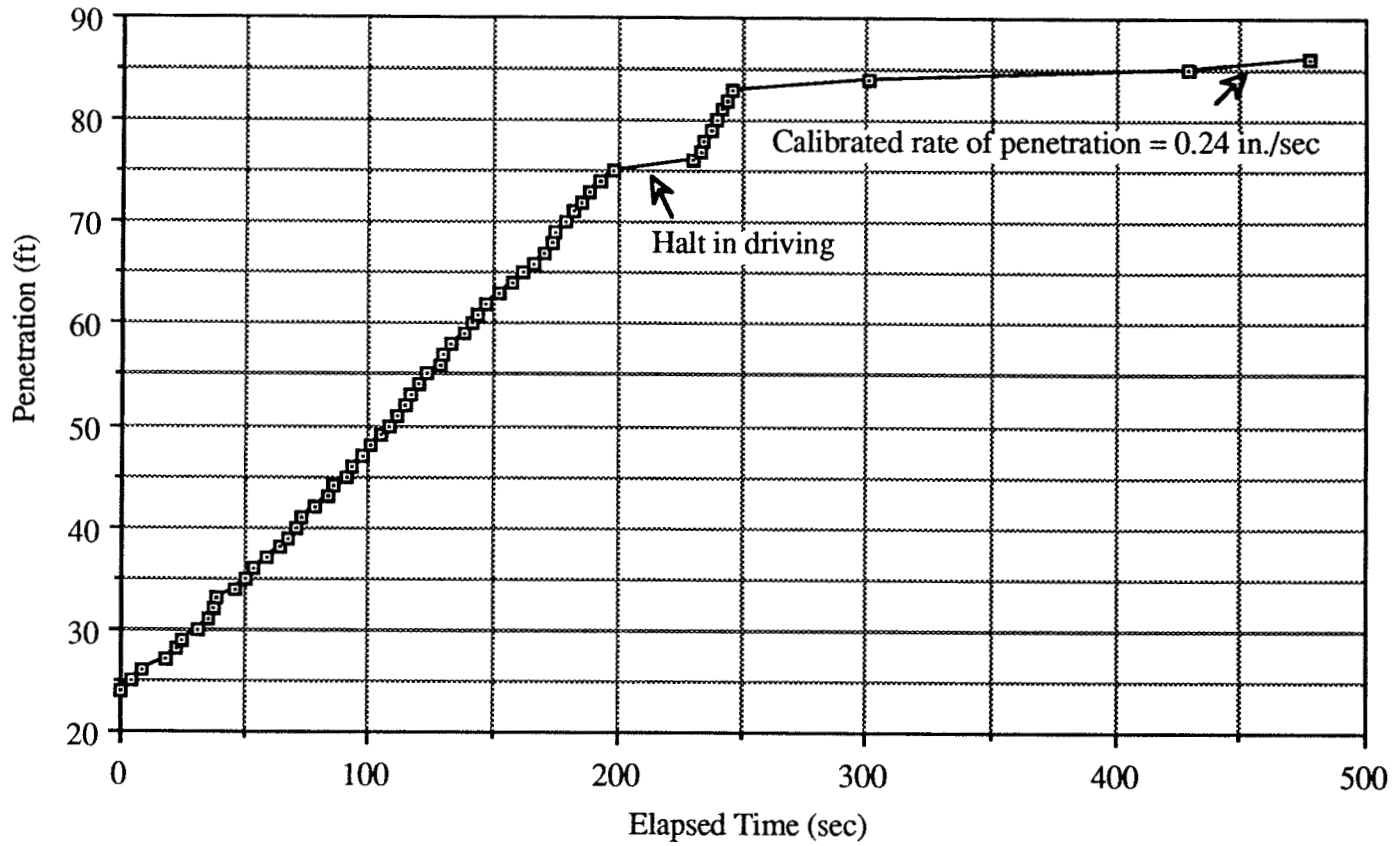


Fig. 3. Rate of Penetration for TP-1

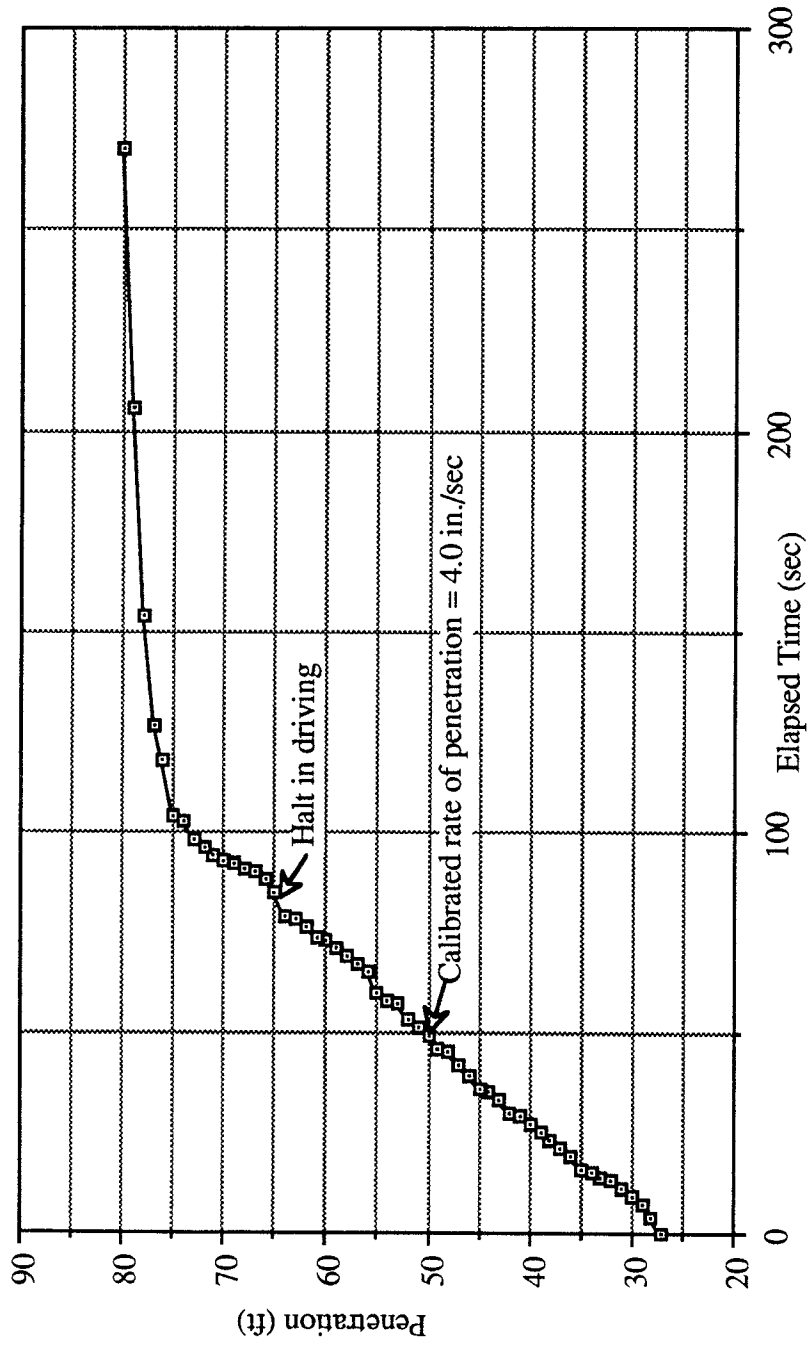


Fig. 4. Rate of Penetration for TP-4

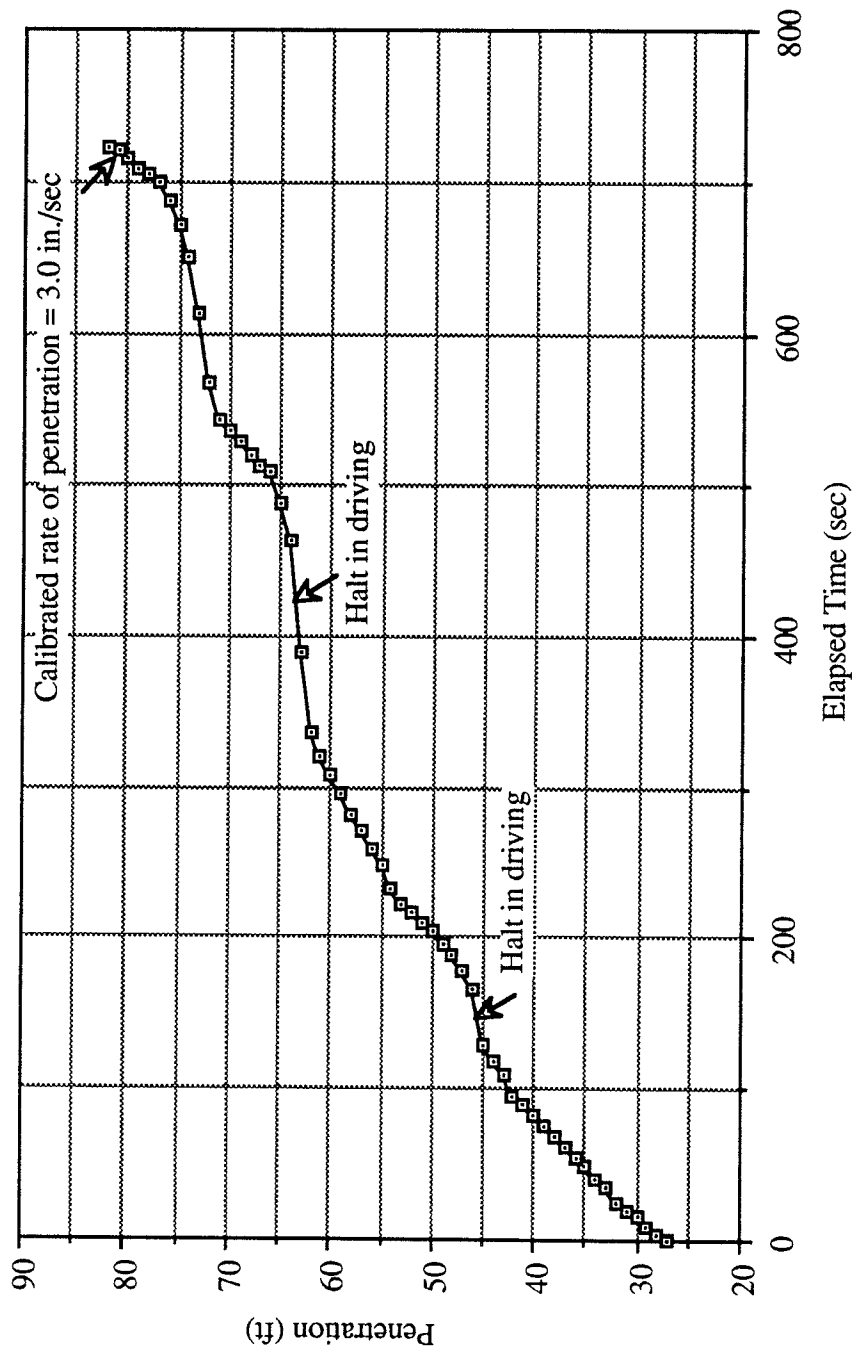


Fig. 5. Rate of Penetration for Pile 559

Uniformly graded, fine, clean siliceous sand, locally termed "San Jacinto River Sand," was placed in the chamber and saturated with deaired water. Drainage was provided at the lateral and upper boundaries of the sand. Controlled effective stresses were maintained at the chamber boundaries during driving and the static loading tests that followed driving. A schematic of the sand column is given in Fig. 6.

To simulate approximately the Pioneer Freezer Site soil conditions, documented in Appendix A, the sand was deposited at 65% relative density throughout the column, and a lateral effective pressure of 10 psi was applied to the submerged sand column. This is not an exact duplicate of the ground conditions at the site. Actual relative density is estimated at 40% above a depth of about 85 feet and 90% below that depth. At the time of the model test, however, methods had not been developed to deposit sand in the testing chamber uniformly at relative densities as small as 40%, so the 65% value represents an average of the relative densities in the upper and lower zones of the Pioneer Freezer Site profile. The mean confining pressure of 10 psi is approximately equal to the mean effective stress in the ground at the middepth of the piles (40 - 44 ft), assuming $K_0 = 0.5$, a total unit weight of 110 pcf and a piezometric surface within 2 ft of the ground surface.

The vibratory driver used in the model study operates on the counterrotating mass principle, as illustrated in Fig. 7. The rotating parts are impelled by hydraulic motors, which are in turn driven by an electric hydraulic pump. The vibrator can be operated in the frequency range of 5 to 50 Hz with unbalanced moments of 35 to 300 in-lb and bias (static) weights ranging from 380 lb to 2000 lb. For these tests the unbalanced moment was 50 in-lb and the biased weight was 380 lb. The theoretical performance curves of the laboratory vibratory driver are shown in Fig. 8. The hammer was connected to the pile head at the weldneck flange by means of a pin and clevice fixture that allowed 0.001 in. tolerance

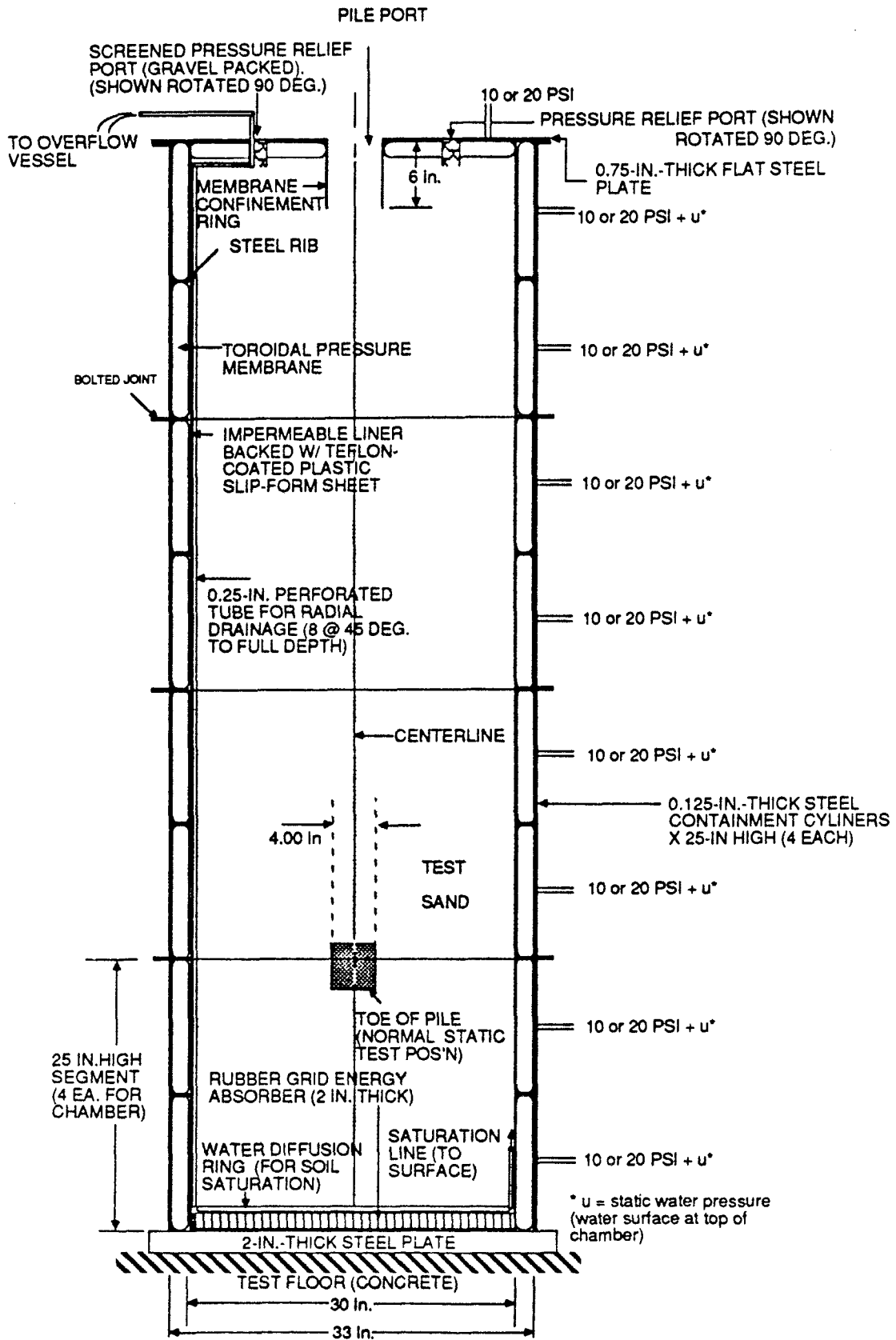


Fig. 6. Detailed Schematic of the Pressure Chamber

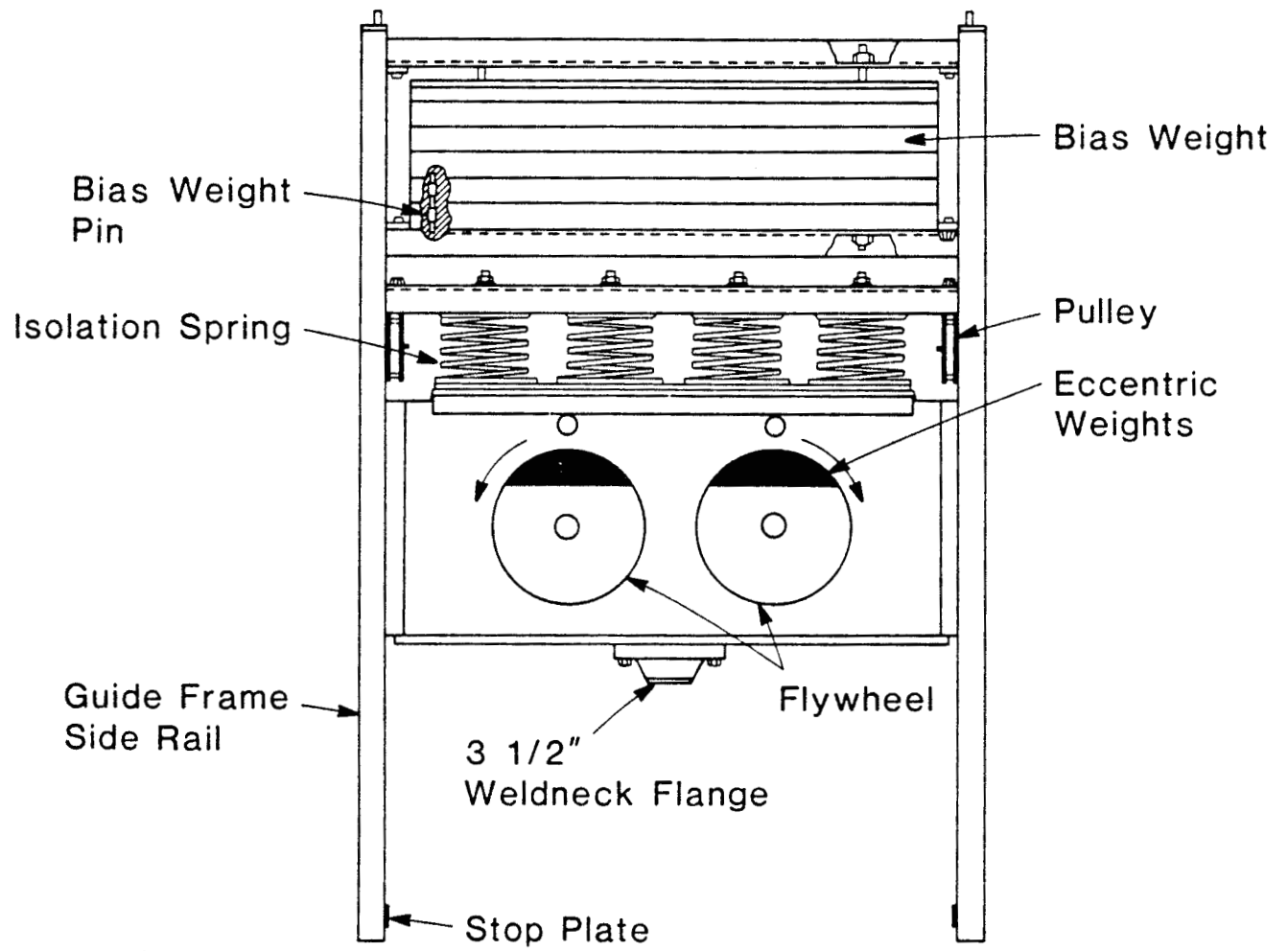


Fig. 7. Schematic Diagram of Vibro-Driver in Laboratory Testing

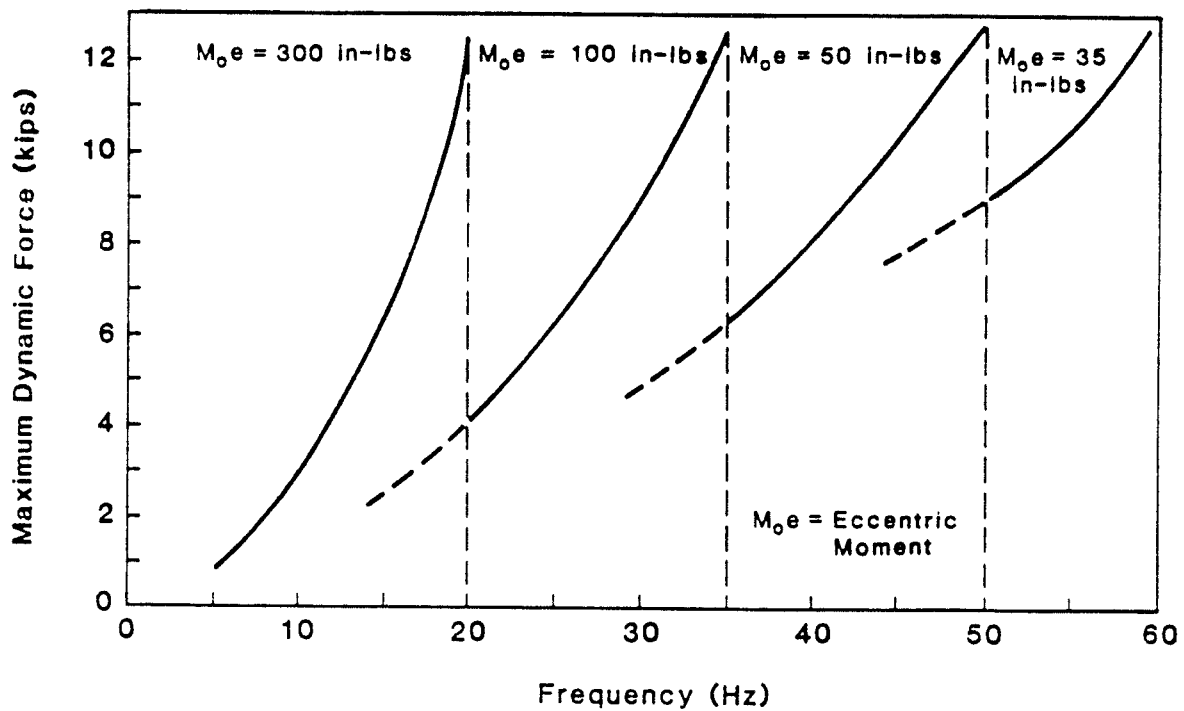


Fig. 8. Theoretical Performance Curves for Laboratory Vibro-Driver

between the pin and the block of the clevice. Some energy losses apparently occurred in this connection, and other energy losses undoubtedly occurred in the hammer itself.

STATIC CAPACITY EVALUATION

TP1 and TP4 were subjected to compressive static loading tests. In general, the test procedure goal was to conduct a 125-ton-maximum loading test (capacity of the dead load reaction), advancing from 0 tons to 125 tons in 10-ton increments. Each increment was held for 10 minutes, with deflection data recorded at the start and at the completion of each increment. At the conclusion of the 50-ton and 100-ton increments the load was dropped to zero and held for 30 minutes. The test was then restarted, the goal being to advance through the remaining increments to 100 or 125 tons. Upon reaching 125 tons the load was held for one hour and unloaded to 100, 75 and 0 tons. TP1 and TP4 were found to have failed at 90 tons and 56 tons, respectively, according to the Offset (Davisson) Failure Criterion. Load-settlement relations are shown for TP1 and TP4 in Figs. C17 and C18, in Appendix C.

Production piles 559, 619, 691, 754 and 825 were restruck and dynamically tested by a PDA. They were not subjected to static loading tests. The hammer used for the restrike was a double acting diesel hammer (ICE 440). The maximum recorded resistance was based on the Case Method of capacity evaluation.

The two model piles were also subjected to compressional static loading tests after they were vibrated to the penetration of 78 in. in the chamber. These tests were monotonic constant rate of penetration tests, conducted at a movement rate of 0.03 in./min. Capacities were interpreted from these loading tests, also using the offset method. Load-settlement curves are shown in Figs. D9 and D10, in Appendix D.

Table 1 gives the interpreted capacities of all test piles and production piles at the Pioneer Freezer Site and of the two model piles tested at UH. The method of failure load determination (loading test or PDA analysis) is indicated.

Table.1 Interpreted Pile Capacities at Pioneer Freezer Site
(compiled from data provided by GZA (5))

Pile #	Observation	Capacity (tons)
TP1	Load tested to failure	90
TP2	Dynamic test (PDA)	106.5
TP3	Load tested with no failure	125
TP4	Load tested to failure	56
TP5	Dynamic test (PDA)	86.5
TP7	Problems with hammer	N/A
559	Dynamic test (PDA)	60
619	Dynamic test (PDA)	62
691	Dynamic test (PDA)	70
754	Dynamic test (PDA)	75
825	Dynamic test (PDA)	70
2A - Model	Load tested to failure	7.20
7C - Model	Load tested to failure	3.75

Notes: Boldface indicates piles that were driven by vibration. Only Piles TP1, TP4, 559, 2A and 7C were analyzed.

TEST RESULTS

Recorded data were reduced to engineering units after being digitized. Plots of top force and accelerations for small time windows, generally smaller than 1 second, have been

generated from the field or lab data for pile penetrations of less than one diameter or width from final penetration for lab tests. The digitized accelerations were corrected for zero shift and then integrated. Zero shift corrections were applied to the field accelerometer data by adjusting the zero until the area under the positive and negative portions of the acceleration-time relation were equal over the time window used. The velocity time histories obtained from the integration of the corrected acceleration time histories were also corrected to account for the constants of integration and so that their integrals would yield displacement-time histories approximately equal to the displacement time histories recorded visually by the video camera. The trapezoidal rule was used for integration. Representative graphs are shown in Appendix C (for the full-sized piles) and Appendix D (for the model piles). As shown in Fig. C6a, the force signal was very noisy for TP4, so very small time windows were selected for the analysis of the data for TP4 (Figs. C6 - C8).

The correction process yielded mean displacement time histories that approximated the observed rate of penetration except in the case of very slow penetration (e. g., TP1). For such a case, very small errors in either the acceleration readings or the zeroes for those readings lead to large percentage errors in computed displacement time history, and no further simple data manipulation can be performed. However, the effect of such errors on velocity time histories is small, so that the peak-to-peak velocities can be used as a checking parameter in the wave-equation optimization process, described subsequently.

WAVE EQUATION ANALYSIS

General

The implementation of one-dimensional wave propagation theory in a finite difference numerical scheme to solve pile driving problems is attributed to Smith (3). Practical refinements of the simplified solution of Smith (e. g., 1, 2) have had a major impact on the state of the art of pile driving. Figure 9 depicts Smith's rheological model of

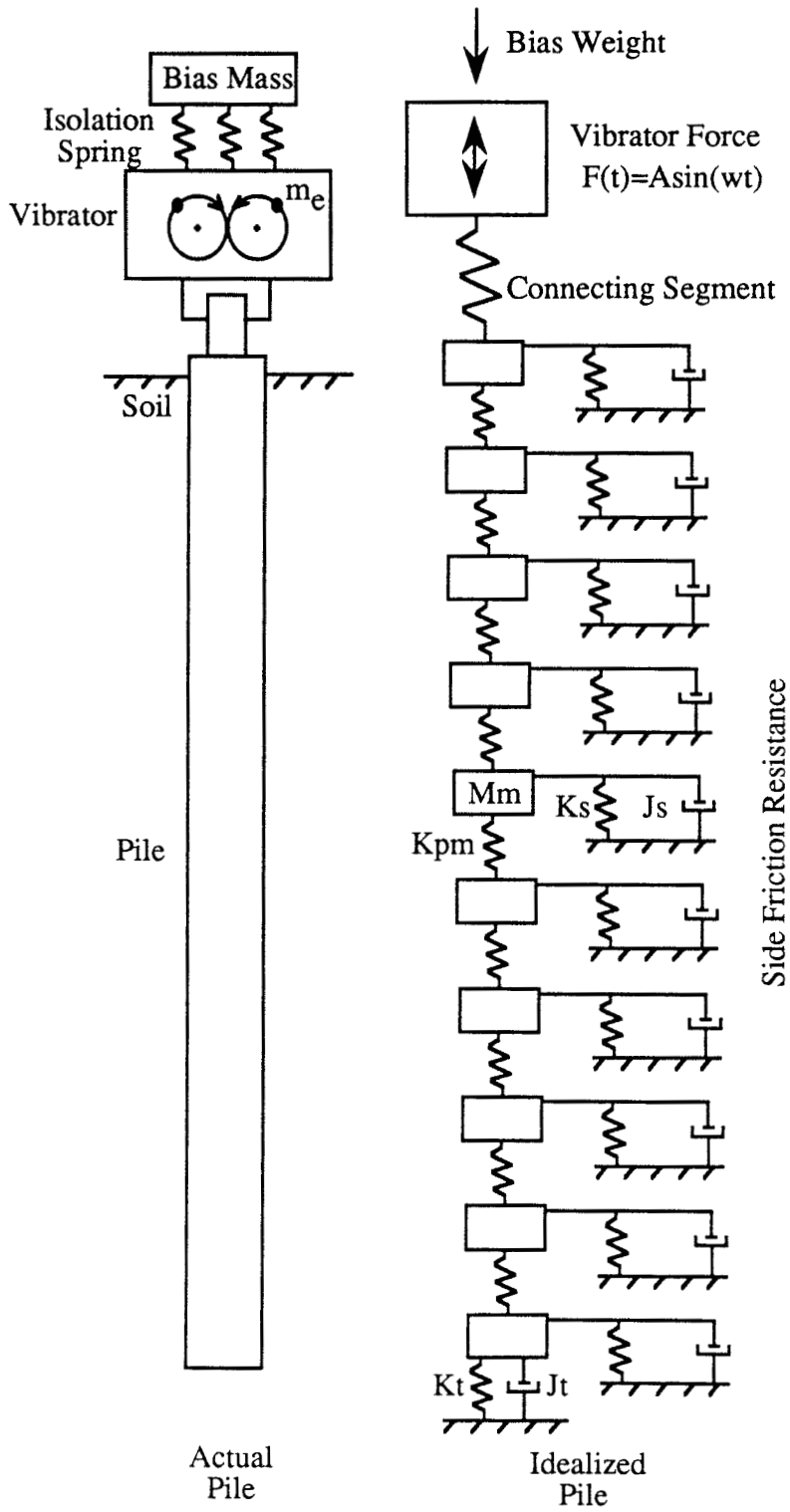


Fig. 9. Lumped Mass System

the problem, in which the pile is discretized into lumped masses connected by springs and the soil-pile interactions similarly represented by a series of (nonlinear) springs and dashpots. Modifications necessary to model the vibro-driving of piles were made as follows:

(1) A version of the wave equation program was written in which the hammer / cushion system found in an impact-driven pile was replaced by a sinusoidal forcing function. In this way a close approximation of the measured force time history could be applied as a pile-head boundary condition that would allow back-computation of the Smith soil parameters without the need to estimate energy dissipation characteristics of the hammer and the hammer-pile connection.

(2) A version of the program was also written that will simulate the mechanical action of the vibratory driver and connection (Fig. 9a). This version was used to reanalyze the field and model piles after the optimum Smith soil parameters had been developed using the first version of the program by freely varying the power dissipation characteristics of the hysteretic connector spring until close compliance was achieved between computed and measured pile-head forces. This exercise was conducted only for TP1.

In this particular study, the soil model employed was the Smith model that is commonly used for modelling of impact driving. It is an elasto-plastic soil model characterized by ultimate static resistance, a quake value and a damping factor (3). Since this model is familiar to the engineering community at large, it will be very beneficial to determine whether it could in fact predict the behavior of vibro-driven model piles.

Formulation of the Wave Equation for Cyclic Force Analysis (Mod. 1)

A sinusoidal force generated by the vibrator acts on the head of the pile as it is pushed down into the ground. Because the pile response cannot be modelled correctly

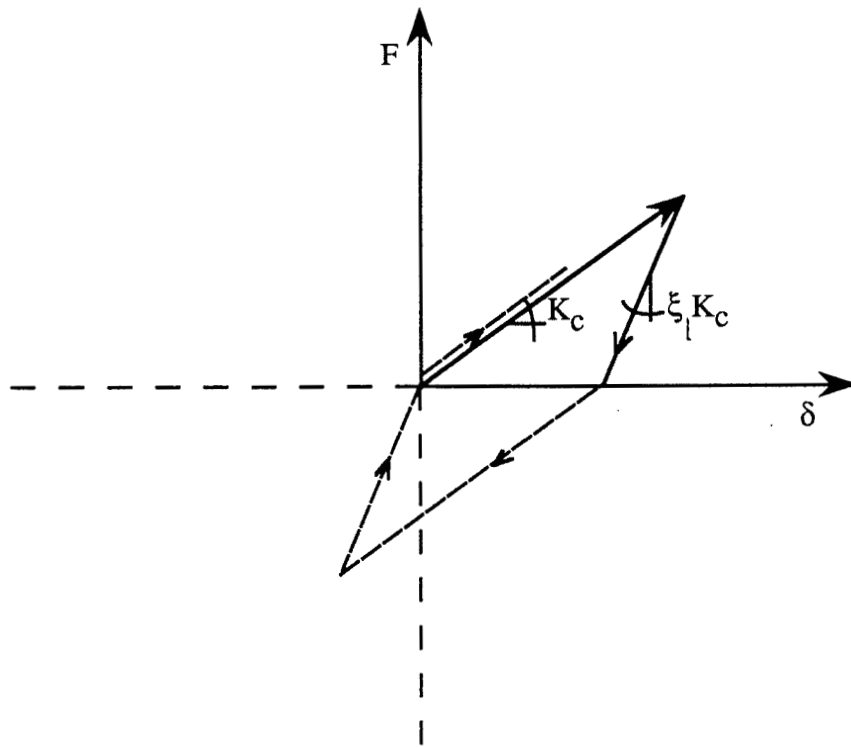


Fig. 9a. Rheological Model of Connecting Segment

without quantifying the energy losses at the pile-vibrator connection, it is not appropriate to determine the Smith soil parameters from a model that includes the vibratory driver in the system. Instead, the sine force measured at the pile head is used as the driving input function.

Forward difference integration with a small time step is started from the time the vibro-driven pile is in its virtual final position and vibro-driving is simulated for 15 to 20 cycles of load, or until steady state penetration is achieved. Output from this scheme, summarized below, includes displacement time history at the pile head, velocity time history at the pile head and static capacity.

Pile-Head Velocity. The pile-head velocity is computed from Eq. 1:

$$V_{1,i} = V_{1,i-1} + [F(i) - F_{1,i-1} - R_{1,i-1}] \frac{\Delta t}{M_1} \quad , \quad (1)$$

where $F(i)$ is the applied pile-head force at time step i and $F_{1,i-1}$ is the spring force (see continuity calculations, below) acting on the bottom of pile element 1 during the previous time increment.. $R_{1,i-1}$ is shaft soil resistance force (see below) developed against element 1 at time step $i-1$. Note that the first computation made to initiate the solution is for $V_{1,1}$. In that case, $R_{1,0}$ and $F_{1,0}$ are zero. Δt is the time increment, and M_1 is the mass of element 1.

Continuity Calculations. The displacements at every time increment i for every pile element m is given by

$$D_{m,i} = D_{m,i-1} + V_{m,i-1} \Delta t \quad . \quad (2)$$

The pile spring compression or tension, C , between elements m and $m+1$ is calculated from:

$$C_{m,i} = D_{m,i} - D_{m+1,i-1} \quad , \quad (3)$$

which in turn gives the spring force in pile, F , at the location of the spring by:

$$F_{m,i} = C_{m,t} K_{pm} \quad , \quad (4)$$

where K_{pm} is the spring constant for pile element $m = \frac{AE_m}{L_m}$, where AE_m is the elastic stiffness of element m and L_m is the length of element m .

Velocities for elements other than Element 1. The velocity for any pile element other than element 1 is given by Eq. 5:

$$V_{m,i} = V_{m,i-1} + [F_{m-1,i} - F_{m,i} - R_{m,i-1}] \frac{\Delta t}{M_m} \quad (5)$$

Note that at the bottom of the pile (element M), $R_{M,1-1}$ is the sum of the shaft and toe resistances.

Shaft Resistance. The shaft resistance force, R , at element m is given by:

$$R_{m,i} = [D_{m,i} - DP_{m,i}] K_s (1 + J_s V_{m,i}) \quad , \quad (6)$$

where DP is the plastic displacement of the soil (displacement in excess of the shaft quake, Q_s), J_s is the side damping constant of soil in units of $\frac{T}{L}$, and K_s is the shaft soil spring constant ($\frac{Q_s}{R_{um}}$, where R_{um} is the ultimate static shaft resistance assigned to element m).

Toe Resistance. The toe resistance function is given by

$$R_{M,i} = [D_{M,i} - DP_{M,i}] K_t (1 + J_t V_{M,i}) \quad , \quad (7)$$

where K_t is the soil spring constant at the toe ($\frac{Q_t}{R_{ut}}$, where Q_t is the toe quake and R_{ut} is the ultimate static toe resistance) and J_t is the toe damping constant.

The loading and unloading paths for the soil are depicted in Figs.10 and 11 for toe resistance and shaft resistance, respectively. Note that no negative (tensile) forces that might be computed by Eq. 7 are permitted at the toe. Furthermore, reloading at the toe cannot commence until the displacement at the end of the most recent unloading cycle has been reached.

A Fortran computer code was developed that incorporates the equations given above through modular subroutines. The unknowns are systematically evaluated from the head of the pile (element 1) to the toe (element M) from time step 1 through a sufficient number of time steps to describe several cycles of loading. The order of solution is repetitively from Eq. 1 or 5 through Eq. 7 (skipping Eq. 1 and using Eq. 5 for $m \neq 1$, and skipping Eq. 5 for $m = 1$) for each time step, with allowances for the constraints on the soil loading paths indicated in Figs. 10 and 11. The code was tested for mathematical stability over as many as 30 cycles of vibration. At least 10 cycles of steady state response at constant rate of penetration were considered necessary for the solution to be considered stable. This means that 15 to 20 cycles must be simulated in order to damp out initial transients. An initial concern for the multi-cycle analysis was the solution stability, but the Eulerian integration method in the time domain, outlined above, proved satisfactory given an appropriate choice of the time step of integration, which, after investigation, was taken as one-half the time required for a compression wave to traverse the shortest pile element. That is, $\Delta t = \frac{L_m(\min)}{2v_c}$, where v_c is the compression wave velocity of the pile material.

Formulation of the Wave Equation for Analysis with Vibrator (Mod. 2)

For this case the analysis of the pile is identical to that in the previous case except that Eq. 1 is not used for element 1 and $F_{0,i}$ in Eq. 5 becomes the force in the connector spring at time increment i . An additional mass, M_0 , is added above element 1 to represent

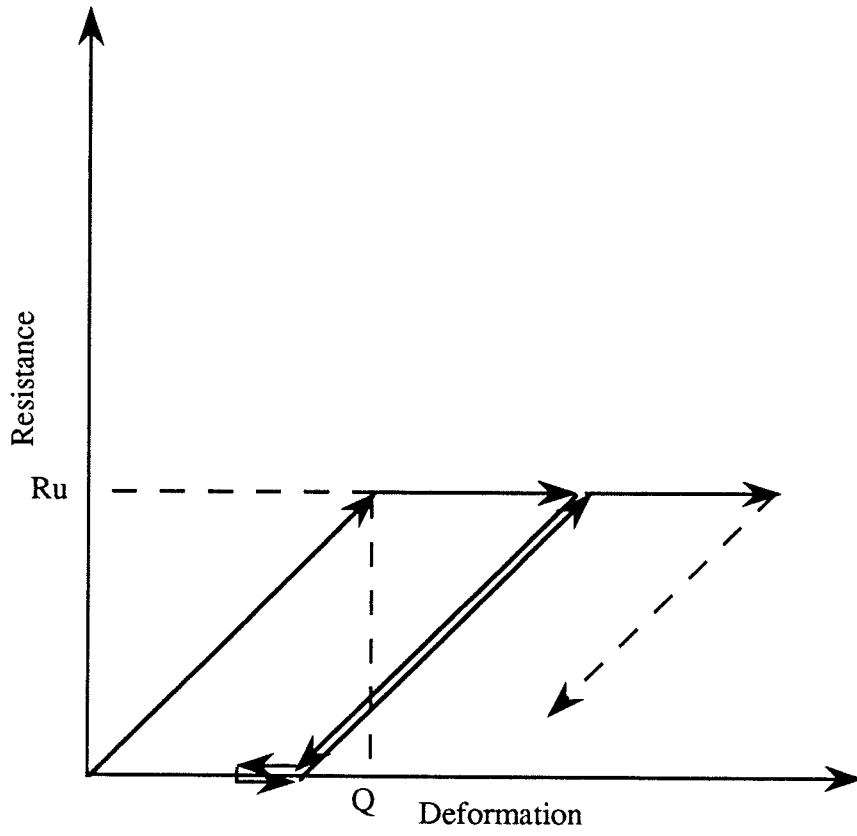


Fig. 10. Toe Soil Loading-Unloading Pattern

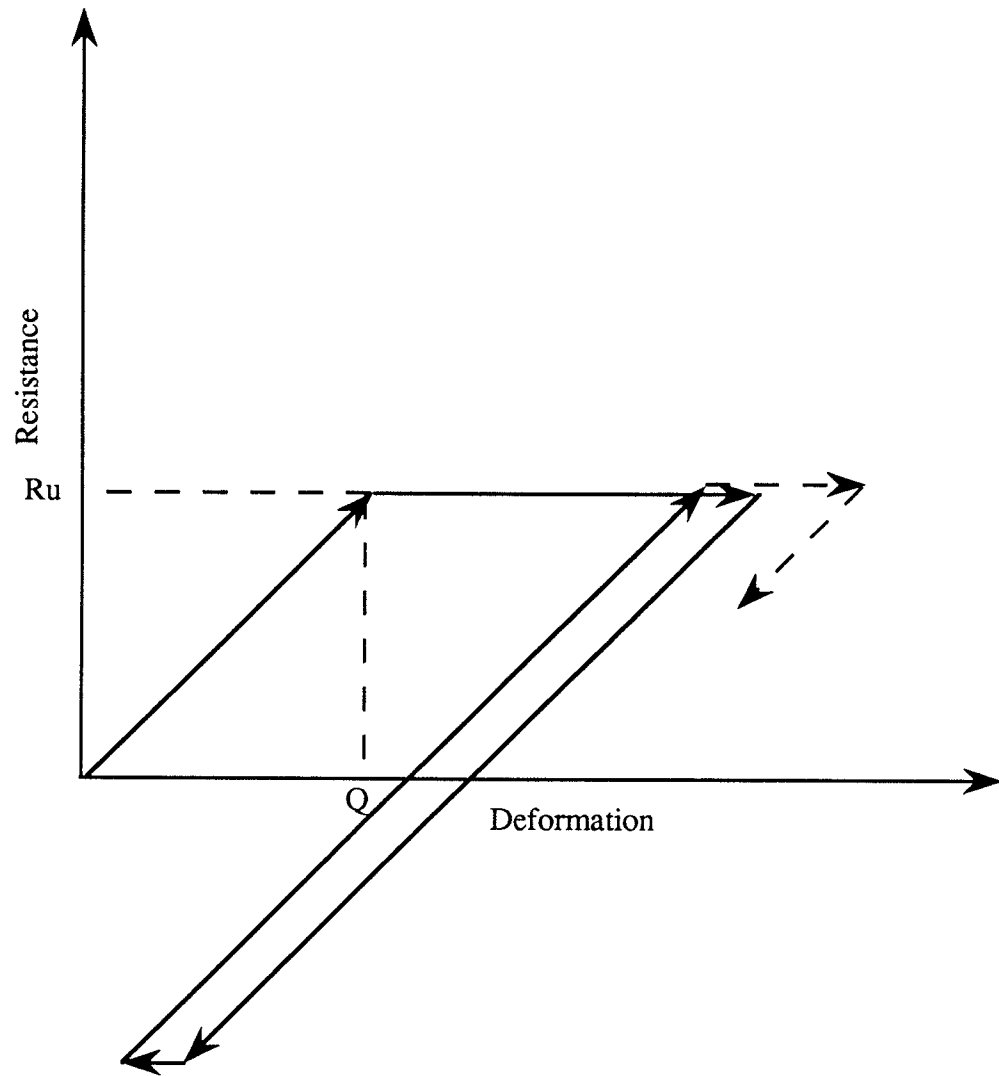


Fig. 11. Shaft Soil Loading-Unloading Pattern

the mass of the hammer. Two forces, the sinusoidal force produced by the counterrotating masses in the hammer and a static force representing the bias weight are considered in the dynamic equilibrium for this new element, as follows. First, the theoretical forcing function for the vibrator, $F_v(t)$, is given by

$$F_v(t) = m_e e (2\pi f)^2 \sin [(2\pi f) t] = A \sin \omega t \quad (\text{Fig. 9}), \quad (8)$$

which, because of internal energy losses in the vibratory hammer, can be modified to

$$F_{0,i} = \xi_2 m_e e (2\pi f)^2 \sin [(2\pi f) t] = \xi_2 A \sin \omega t \quad (\text{Fig. 9}), \quad (8a)$$

where m_e is the magnitude of the combined eccentric masses in the vibrator, e is the moment arm of these masses, f is the operating frequency of the vibrator in Hz, ξ_2 is an empirical energy loss term, and the first subscript (0) represents the vibrator mass. Then

$$V_{0,i} = V_{0,i-1} + [F_B - F_{0,i-1} + F_v(t)_i] \frac{\Delta t}{M_0}, \quad (9)$$

in which M_0 is the mass of the vibrator, excluding the bias weight, F_B is the value of the bias weight and $F_{0,0}$ and $V_{0,0}$ are 0. With $V_{0,i}$ known,

$$D_{0,i} = D_{0,i-1} + V_{0,i} \Delta t, \quad (10)$$

$$C_{0,i} = D_{0,i} - D_{1,i-1}, \quad \text{and} \quad (11)$$

$$F_{0,i} = \alpha K_c C_{0,i}. \quad (12)$$

In Eq. 12, $\alpha = 1$ if $C_{0,i} > C_{0,i-1}$ and $C_{0,i}$ is + (compressive),

$\alpha = \xi_1$ if $C_{0,i} < C_{0,i-1}$ and $C_{0,i}$ is +,

$\alpha = 1$ if $C_{0,i} < C_{0,i-1}$ and $C_{0,i}$ is -, and

$\alpha = \xi_1$ if $C_{0,i} > C_{0,i-1}$ and $C_{0,i}$ is -, in order to model the hysteresis (energy losses) in the connection.

K_c is $\frac{AE}{L}$ for the connecting segment, assumed semi-arbitrarily to be a (weightless) two-foot-long steel rod with a cross-sectional area of 12 in². A + value for $C_{0,i}$ indicates compression, while a - value indicates tension in the connection.

Energy losses in the hammer and connection in this scheme are modelled by two parameters, ξ_1 , which models empirically the hysteresis in the connector spring, and ξ_2 (Eq. 8a), which models empirically the internal energy losses in the hammer. As further research is conducted into energy losses in vibratory driving systems, more appropriate energy loss expressions can be developed.

Once $F_{0,i}$ is computed in a given time step, computations proceed for pile elements 1 - M for that time step as in Modification 1. If the toe and shaft resistance, quake and damping are known (as, for example, from an optimization of the parameters from the use of a measured forcing function at the pile head), ξ_1 and ξ_2 are the only free variables, and they can be evaluated in principle by varying ξ_1 and ξ_2 in a complete analysis of the pile-vibrator-soil system. The soil parameters are held constant and ξ_1 and ξ_2 are varied until (a) the force time history $F_0(t)$ approximates the forcing function at the pile head that was measured experimentally, as indicated in Fig. 12 (which shows specific data for the simulation of TP1) and (b) simultaneously there is a close match in the predicted and measured rates of pile penetration.

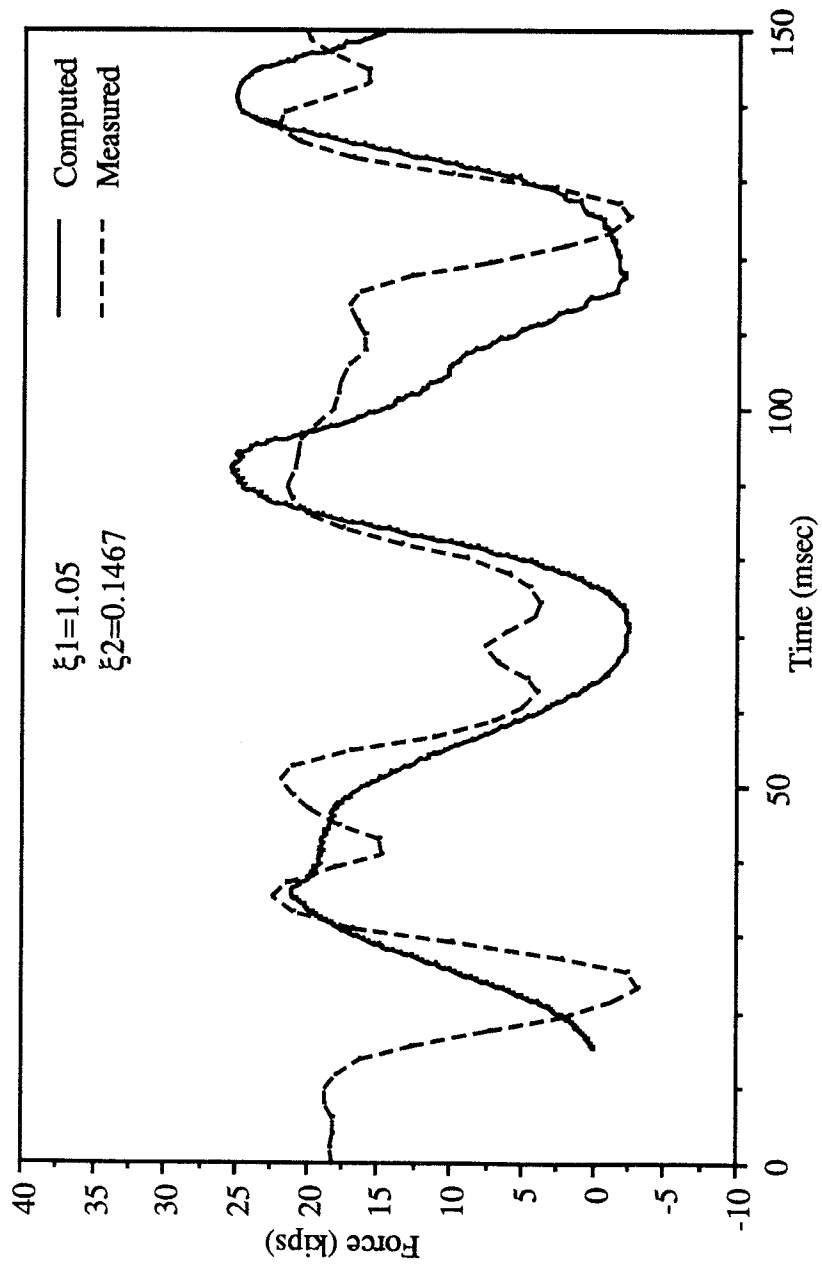


Fig. 12. Pile-Head Force vs Time for TP-1

OPTIMIZATION OF PARAMETERS

First Stage Optimization

Systematic numerical simulation of both the field and lab tests was undertaken using the Smith soil model in the numerical solution (Modification 1). By considering the measured pile-head driving force time history as input in the wave equation code and by minimizing both the error in rate of penetration v_p and the peak-to-peak pile-head velocity $v_{1,pp}$ at within one diameter of full penetration (through comparison with measured values), the ultimate resistance (capacity), ratio of toe resistance to total resistance and the Smith parameters were obtained for each pile installation that was simulated. Many computer runs were necessary to optimize all parameters for a given test.

For purposes of analysis, the laboratory test piles were divided into two elements because the piles were short enough to behave almost as rigid bodies. TP1, TP4 and Pile 559 on the other hand were divided into five elements to account for the greater flexibility of the full-sized piles.

An optimization matrix is shown schematically in Table 2, which illustrates how the optimization process was carried out. Note that in this optimization procedure the assumption was made that the shaft resistance was constant along the pile.

The results of this optimization procedure are given in Tables 3 through 7. It is noted that the solution for TP4 could not be optimized at full penetration, since pile-head velocity records were not found for that penetration, so that optimization was performed for the deepest penetration for which data were available (50 ft). As a result, no comparison between computed and measured capacity could be obtained for that pile.

Table 2. Schematic Optimization Matrix for Wave Equation Analyses (Mod. 1)

Run	Free Variables						Computed Variables	
	R_{uT}	$\frac{R_t}{R_{uT}}$	Q_s	J_s	Q_t	J_t	v_p	$v_{1,pp}$
1	X	X	X	X	X	X	Y	Z
2	X	X	X	X	X	X	Y	Z
...
N	X	X	X	X	X	X	Y	Z

Optimum set of parameters occur where

$$\min \{ [Y - v_p(\text{measured})]^2 + [Z - v_{1,pp}(\text{measured})]^2 \}^{0.5}$$

is obtained.

Table 3. Optimized Pile and Soil Parameters for TP1

Parameter	Value
Q (shaft)	0.05 in.
Q (toe)	0.15 in.
J (shaft)	0.020 sec/in.
J (toe)	0.042 sec/in.
R_{uT} (total ult. resistance)	12.5 tons
$R_{ut}(\text{toe}) / R_{uT}(\text{total})$	0.50
R_{uT} / R_{uT} (loading test)	0.14

Table. 4. Optimized Pile and Soil Parameters for TP4
(Based on data for 50-ft penetration)

Parameter	Value
Q (shaft)	0.05 in.
Q (toe)	0.15 in.
J (shaft)	0.004 sec/in.
J (toe)	0.008 sec/in.
R_{uT} (total ult. resistance)	3.75 tons
$R_{ut}(\text{toe}) / R_{uT}(\text{total})$	0.30
R_{uT} / R_{uT} (loading test)	Not obtainable

Table. 5. Optimized Pile and Soil Parameters for Pile 559

Parameter	Value
Q (shaft)	0.05 in.
Q (toe)	0.15 in.
J (shaft)	0.020 sec/in.
J (toe)	0.042 sec/in.
R_{uT} (total ult. resistance)	4.5 tons
$R_{ut}(\text{toe}) / R_{uT}(\text{total})$	0.30
R_{uT} / R_{uT} (loading test)	0.08

Table. 6. Optimized Pile and Soil Parameters for Pile 2A (Lab)

Parameter	Value
Q (shaft)	0.05 in.
Q (toe)	0.15 in.
J (shaft)	0.021 sec/in.
J (toe)	0.067 sec/in.
R_{uT} (total ult. resistance)	2.1 tons
$R_{ut}(\text{toe}) / R_{uT}(\text{total})$	0.55*
R_{uT} / R_{uT} (loading test)	0.29

* Note: During static loading test, this ratio was 0.38

Table. 7. Optimized Pile and Soil Parameters for Pile 7C (Lab)

Parameter	Value
Q (shaft)	0.05 in.
Q (toe)	0.15 in.
J (shaft)	0.021 sec/in.
J (toe)	0.067 sec/in.
R_{uT} (total ult. resistance)	1.13 tons
$R_{ut}(\text{toe}) / R_{uT}(\text{total})$	0.30
R_{uT} / R_{uT} (loading test)	0.30

Second Stage Optimization

Using the parameters in Table 3, TP1 was analyzed again using Modification 2 of the wave equation program in order to evaluate the energy dissipation parameter ξ that will

enable the entire hammer-pile-soil system to be simulated. The values of ξ_1 and ξ_2 that gave the closest correspondence between measured and predicted force time history at the pile head at maximum penetration in TP1 were 1.05 and 0.147, respectively. These data suggest little power loss in the connector but a hammer "efficiency" of only about 15%.

SENSITIVITY STUDY

A sensitivity analysis was conducted for Pile 2A (laboratory test pile) using Modification 1 of the wave equation program by changing only one optimum test parameter at a time, keeping the other optimized test parameters unchanged. Plots of rate of penetration and peak-to-peak pile head velocity versus changing quake (shaft and toe), soil damping (shaft and toe), ratio of toe to shaft resistance, and static pile capacity in flight (R_{uT}) are shown in Appendix E. Penetration rate and head velocity are both seen to be rather sensitive to the choice of some of the parameters. Both penetration rate and peak-to-peak head velocity were more sensitive to R_{uT} , the total static capacity, and to J_t , the damping constant assigned to the pile toe, than to variations in the other variables, within a range of $\pm 50\%$ of the computed optimum value. The high degree of sensitivity of R_{uT} to penetration rate is encouraging for the use of wave equation modelling to predict static capacity. However, the sensitivity of the solution to J_t suggests that more back-analyses, particularly of field installations, or more refined methods for predicting J_t theoretically, or both, will have to be acquired before wave equation modelling can be used with confidence for this application.

Another variable that has a significant effect on rate of penetration, but less so for peak-to-peak velocity, is ratio of toe to total resistance. During the static test on 2A the toe resistance was measured by means of a load cell and was found to be 0.38 X total capacity. compared with 0.55 inferred from the wave equation optimization process. This suggests that a fair approximation of the R_t/R_{uT} can be obtained from application of static pile

capacity theory. (This is obviously not true, however, for the absolute value of R_{uT} .) The fact that R_v/R_{uT} was nearly equal for Test 2A (lab) and TP1(field) seems, on first consideration, fortuitous, since L/B for TP1 was about four times that for 2A, which would suggest a lower ratio for TP1. However, the soil at the toe of TP1 was much stronger than the soil along the shaft, which was not the case in the laboratory. Hence, as a first trial, the use of static capacity ratios appears possible for vibratory driving modelling.

CONCLUSIONS

The following conclusions can be drawn from this preliminary study.

1. The wave equation program with the Smith soil model and conventional Eulerian integration can be used to predict the behavior of piles driven by vibration. It must be applied by simulating the driving of the pile, starting from a static position near full penetration, for about 15-20 cycles, to clear initial transients and to achieve about 10 cycles of steady-state motion of the pile head. Other soil models, however, may provide better predictions than the Smith model. Research is continuing at the University of Houston.

2. In order to model the hammer-pile-soil system, the following properties of the hammer and connection to the pile must be known: weight of rotating parts, moment arm of rotating parts, frequency of operation, weight of vibrator body, magnitude of bias weight, and the energy dissipation constants ξ_1 and ξ_2 . The former parameters can be obtained from hammer manufacturers, while ξ_1 and ξ_2 must be obtained experimentally. Values of ξ_1 and ξ_2 for Pile TP1 (with ICE 416 driver) have been suggested in this report, but those values should not be generalized without further study. Other means of characterizing power losses in the hammer and at the pile-hammer connection may be more appropriate than the method described in this preliminary study. The stiffness of the connector may also be an important variable. This effect was not investigated here.

3. In some respects, the tests conducted in the laboratory replicated certain effects that were inferred from wave equation modelling of the field tests at the Pioneer Freezer Site. For example, the values of R_{ut}/R_{uT} were essentially identical between the laboratory and field tests on the pipe pile TP1 (0.50 - 0.55), but a lower ratio (0.30) was achieved for pipe Pile 559. The driving record suggests that the soil in the locality of the toe of Pile 559 was weaker than at the location of TP1, and it is therefore reasonable that R_{ut}/R_{uT} also be lower for that pile. It is suggested that R_{ut}/R_{uT} can be estimated for closed-toe pipe piles from static resistance theory as a first approximation. Further, quake values and shaft damping values were essentially equal among all of the laboratory and field pipe piles.

4. On the other hand, some major differences occurred between the lab and field tests. There was little similarity in the Smith damping values between TP4 and Test 7C (H-piles), although the quake values were equal. This may be due to the fact TP4 could only be analyzed at partial penetration, and that the very rapid rate of penetration at that point permitted significant damping in the hysteresis of the resistance curves, so that relatively

low J-values (similar in magnitude to those that would be used to model impact driving) were appropriate. This observation suggests that a soil model other than the Smith model is desirable. Toe damping was consistently higher for the laboratory model piles than for the field piles. The toe damping differences may be due to differences between the boundary conditions in the chamber and field, especially in the vicinity of the pile toe. Since the prediction of R_{uT} is strongly dependent upon J_t , it is evident that further studies of this type will be necessary to develop with confidence either ratios of $J_t(\text{field})$ to $J_t(\text{lab})$ or confident values of $J_t(\text{field})$ directly. Otherwise, large-scale laboratory tests appear to be a useful tool in developing values for parameters for inclusion in wave equation studies of vibratory pile driving.

5. The most significant difficulty in the modelling process is the prediction of static pile capacity. In every test modelled, R_{uT} (in-flight static resistance) was between only 8% and 30% of the static capacity indicated by the Davisson interpretation of failure from the static load-movement relationship or from analysis of impact restrike data using the Case Method. The vibro-driving process sets up pore water pressures and other phenomena that apparently produce this behavior. In the laboratory the ratios of R_{uT} to static capacity were higher than in the field, possibly because of better drainage. An explicit soil degradation model should therefore be incorporated in the wave equation model. Alternately, it may be possible to obtain better values of static capacities by analysis of penetration rate after the pile is allowed to rest for a few minutes and then vibrated a short distance to final penetration, in a manner similar to the restrike process used in impact driving, but with a much shorter wait time, since soils through which vibro-drive piles penetrate are normally granular and dissipate pore pressures quickly.

ACKNOWLEDGMENTS

The authors express their appreciation to **Mr. William F. Loftus** of William F. Loftus and Associates, who acted on behalf of DFI to acquire the necessary driving and hammer data and to provide those data to the University of Houston, **Mr. William R. Beloff** of GZA and personnel of the **Herbert F. Darling Company** for their attention to the many questions asked during the data reduction operation, **Dr. Reed Mosher** of USAEWES for assistance in transferring data tapes, and to **Parratt-Wolff, Inc.**, and the **New York DOT** for providing geotechnical data for the Pioneer Freezer Site.

REFERENCES

1. Goble, G. G., Rausche, F., and Likins, G. E., "The Analysis of Pile Driving - A State-of-the-Art," paper presented at the First International Symposium on the Application of Stress Wave Theory on Piles, Stockholm, Sweden, 1980.
2. Rausche, F., Moses, F. and Goble, G. G., "Soil Resistance Predictions from Pile Dynamics," *Journal of the Soil Mechanics Foundations Division*, ASCE, Vol.98, No. SM9, Proc. Paper 9220, Sept. 1972.
3. Smith, E. A. L., "Pile Driving Analysis by Wave Equation," *Journal of the Soil Mechanics and Foundations Division*, ASCE, No. 86, August 1960.
4. Goldberg-Zoino and Associates, Inc., *Vibratory Hammer Study Field Measurements*, GZA, Newton Upper Falls, MA, January, 1987.
5. Goldberg-Zoino and Associates, Inc., *Pioneer Freezer Project Dynamic Pile Testing*, Syracuse, New York, GZA, Newton Upper Falls, MA, August, 1989.

APPENDIX A

APPENDIX A

Geotechnical Information

Geology of the Syracuse Vicinity

During the last glacial era, the Syracuse area was covered by a glacial lake. The lake basin, in which the Pioneer Freezer Site is located, was filled with lacustrine silts and clays by underwater sedimentation. These geomaterials have never been subjected to more than their own weight. As the glacial lake and glacier began receding some 10,000 years ago, some of the low areas were occupied by smaller lakes, the present Onondaga Lake, a few hundred yards to the southwest of the site, being one of them.

During the glacial retreat, the areas surrounding Onondaga Lake began being filled by marl, which is a mixture of calcium carbonate, shells, silts and clay. After the marl was laid down, the formation of peat began. The swampy environment, which exists to this day, favored the preservation of the organic material.

In addition to the natural causes of deposition, the foundation conditions are further complicated by man-made deposits. Landfill operations in the Syracuse area have dumped garbage and miscellaneous fill in varying quantities throughout many parts of the area.

Pioneer Freezer Site

The Pioneer Freezer Site, the site where test piles were driven, is located in Onondaga County about three miles northwest of downtown Syracuse, New York. A site location map is shown in Fig. A1.

Scale: 1"=50'

Job Site: Intersection of Park street and Hiawatha Blvd.

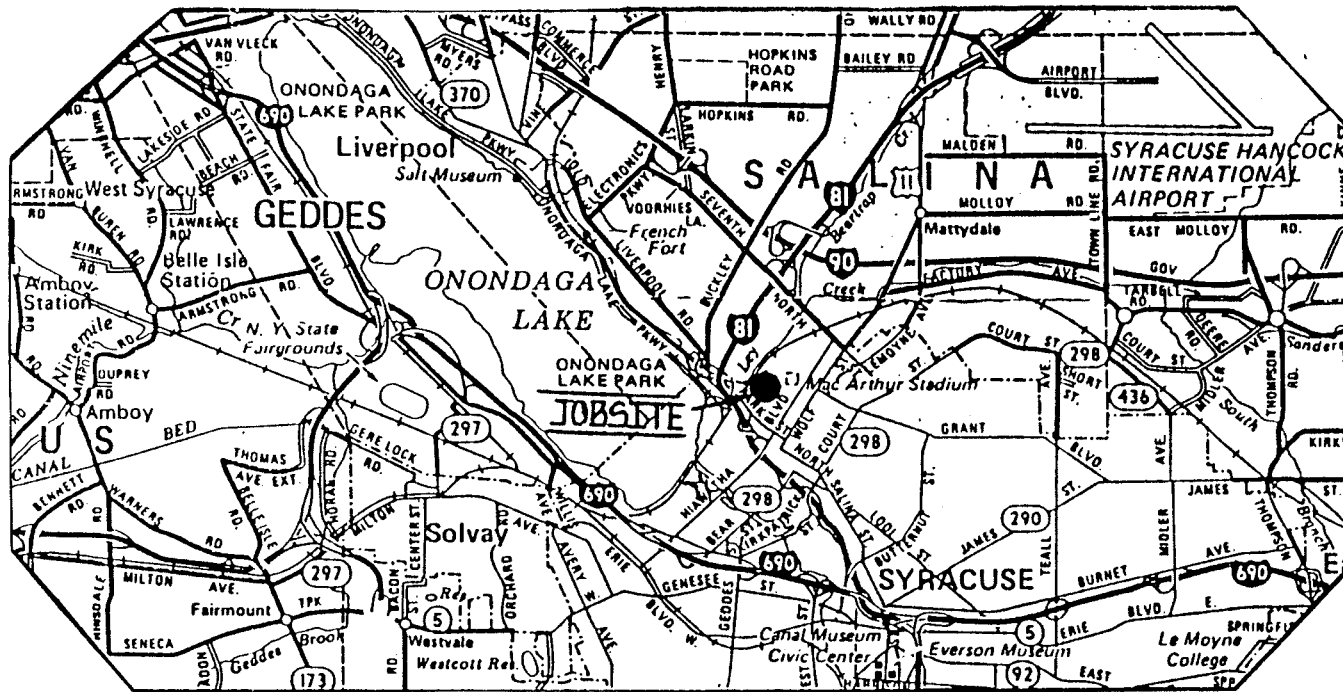


Fig.A1 Site Location Map

Logs of test borings and laboratory tests in and around the testing area were made available by Parratt-Wolff, Inc. The data obtained consist of several boring logs and results of laboratory testing, which include natural moisture content, sieve and hydrometer analyses and Atterberg limits.

In addition, a general subsurface profile for the construction of a Bikeway located 200 feet west of the Pioneer Freezer Site was previously undertaken by the New York DOT and those data could readily be used to assist in characterizing the site.

The existence of the above soil data makes the Pioneer Freezer Site fairly well documented.

The soil information resulting from the test boring closest to the pile driving area, and deep enough to describe the soil stratigraphy up to full penetration of the test piles, constitutes the working soil profile. The standard penetration test was performed in this boring and in adjacent borings according to ASTM-1586. The boring log, showing the uncorrected SPT N values, is presented in Figs. A2 - A4.

It appears that the soil conditions at the testing site consist of an 8 foot-thick of loose cinders and silt fill. This fill is underlain by a 37-foot-thick layer of very soft silt and marl. Underlying this layer are recent alluvial deposits, consisting of silt and medium dense sand, which have been interpreted by the writers to be essentially free draining. The standard penetration resistance (N-values) for the alluvial deposits generally increased with depth to auger refusal. At time of testing, the water table was at the ground surface. From the boring log, it appears also that at the 80-85-foot depth a layer of medium to very dense fine to coarse gravel and fine to coarse siliceous sand with some silt existed. The test piles were driven into this stratum, so that it surrounded the toes of the test piles at their final

DEPTH ▼	SAMPLE DEPTH	SAMPLE NUMBER	C	SAMPLE DRIVE RECORD PER 6"	N	DESCRIPTION OF MATERIAL	STRATA CHANGE DEPTH		
WL	0.0'-	1		1/1		Black wet loose CINDERS and SILT, little fine to coarse sand, little fine to medium gravel			
	2.0'			5/3	6				
5.0	5.0'-	2		1/1					
	7.0'			2/1	3				
10.0	10.0'-	3		1/1				Gray wet very soft MARL	8.0'
	12.0'			1/1	2				
15.0	15.0'-	4		WH/WH					
	17.0'			WH/WH					
20.0	20.0'-	5		WH/1		Gray wet very soft SILT and MARL	20.0'		
	22.0'			1/1	2				
25.0	25.0'-	6		2/1				Gray wet very soft SILT	24.0'
	27.0'			1/1	2				
30.0	30.0'-	7		WH/WH					
	32.0'			WH/WH					
35.0	35.0'-	8		WH/WH					
	37.0'			WH/WH					
40.0									

Fig.A2 Boring Log for 0 to 40' Depth

DEPTH	SAMPLE DEPTH	SAMPLE NUMBER	C	SAMPLE DRIVE RECORD PER 6"	N	DESCRIPTION OF MATERIAL	STRATA CHANGE DEPTH
45.0	40.0'	9		WH/WH		Gray wet very soft SILT	45.0'
	42.0'			WH/WH			
50.0	45.0'	10		4/4		Brown wet stiff SILT	60.0'
	47.0'			5/2	9		
55.0	50.0'	11	NO	6/5		Brown wet medium stiff SILT, some fine sand	63.5'
	52.0'		REC	7/10	12		
60.0	55.0'	12	NO	WH/WH		Brown wet medium dense fine SAND, trace silt	80.0'
	57.0'		REC	3/1	3		
65.0	60.0'	13		3/4		Brown wet medium dense fine SAND, trace silt	80.0'
	62.0'			1/4	5		
70.0	65.0'	14		7/10		Brown wet medium dense fine SAND, trace silt	80.0'
	67.0'			9/9	19		
75.0	70.0'	15		7/9		Brown wet medium dense fine SAND, trace silt	80.0'
	72.0'			14/18	23		
80.0	75.0'	16		6/6		Brown wet medium dense fine SAND, trace silt	80.0'
	77.0'			10/11	16		

Fig.A3 Boring Log for 40' to 80' Depth

penetration depths. At a depth of 82 feet, N is 17 in a medium dense fine sand soil layer. At 86.5 feet, the driller encountered auger refusal.

Geological transformations in the Onondaga County, New York, suggest to the writers that the soil above about 85 feet depth is normally consolidated, while the dense material below that depth is preconsolidated by glaciation. Hence, most of the material through which the piles were driven is normally consolidated, loose and of the free-draining type. This idealization is the result principally of engineering judgment.

APPENDIX B

APPENDIX B

ICE 416 Vibratory Hammer Specifications

The vibro-hammer used to drive the test piles at the Pioneer Freezer Site was an ICE 416. J and M Hydraulics, Inc., who designed the hammer for ICE provided the writers with the following specifications.

Model : ICE 416

Weight: 9600 lb.

Eccentric Moment: 2000 in-lb.

Bias Mass Weight: 3270 lb.

Spring Constant: 15520 lb. per in.

Maximum Extraction Force: 80,000 lb.

Engine Power: 250 HP.

Note that "weight" is the overall weight of the unit, including the bias weight, clamp, and rotating parts. Also the "eccentric moment" is the total of all the unbalanced masses times their eccentricity.

APPENDIX C

APPENDIX C

Typical Driving Data for Pioneer Freezer Site Piles

The following figures show selected segments of the digitized data that were used in this study.

DRIVING HISTORY OF PILE TP-1

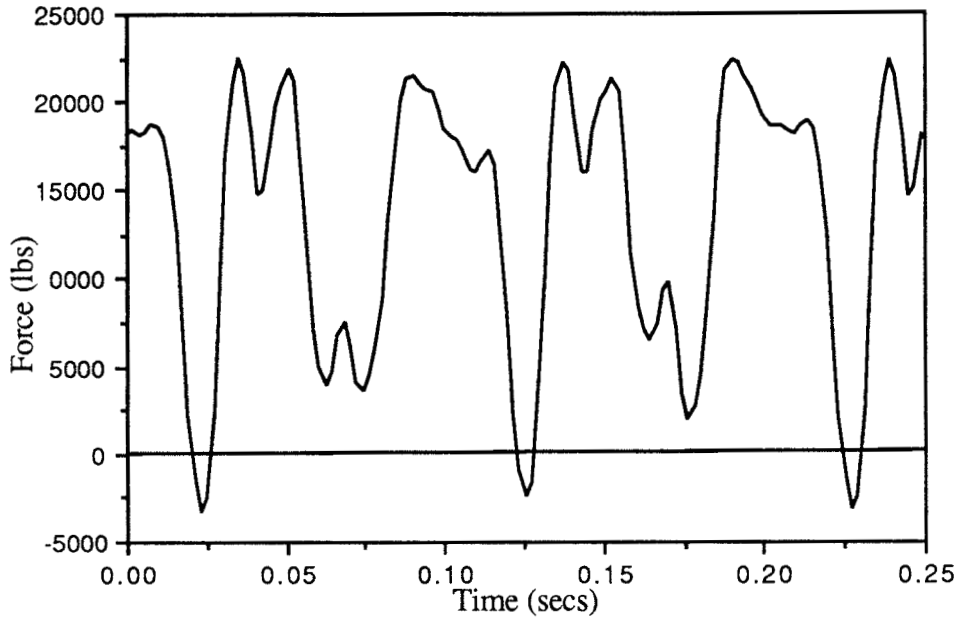


Fig. C1. Pile-Head Force vs Time at 86 ft Penetration Depth

DRIVING HISTORY OF PILE TP-1

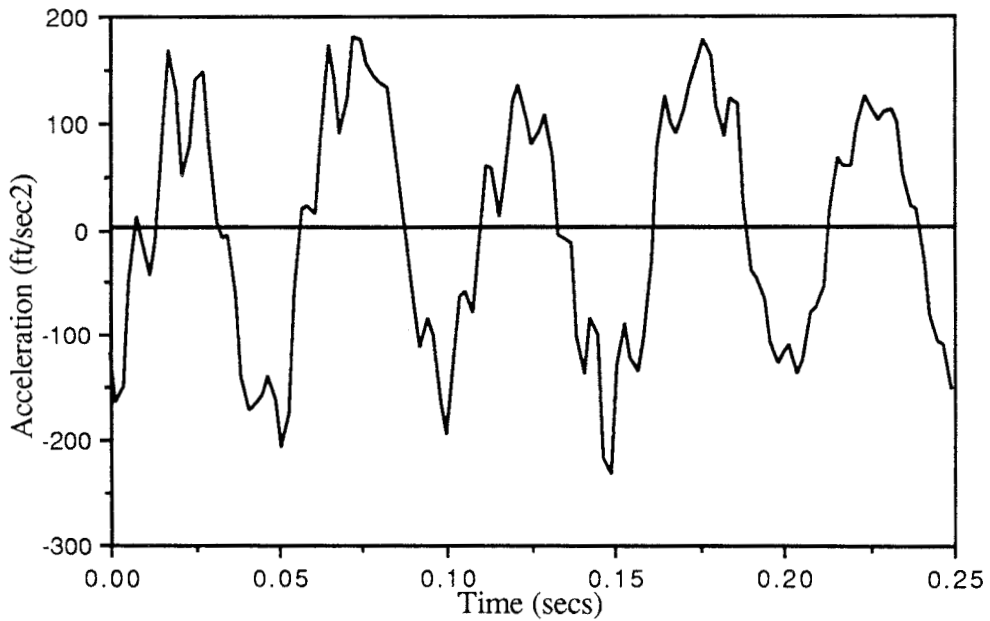


Fig. C2. Corrected Average Pile-Head Acceleration vs Time at 86 ft Penetration Depth

DRIVING HISTORY OF PILE TP-1

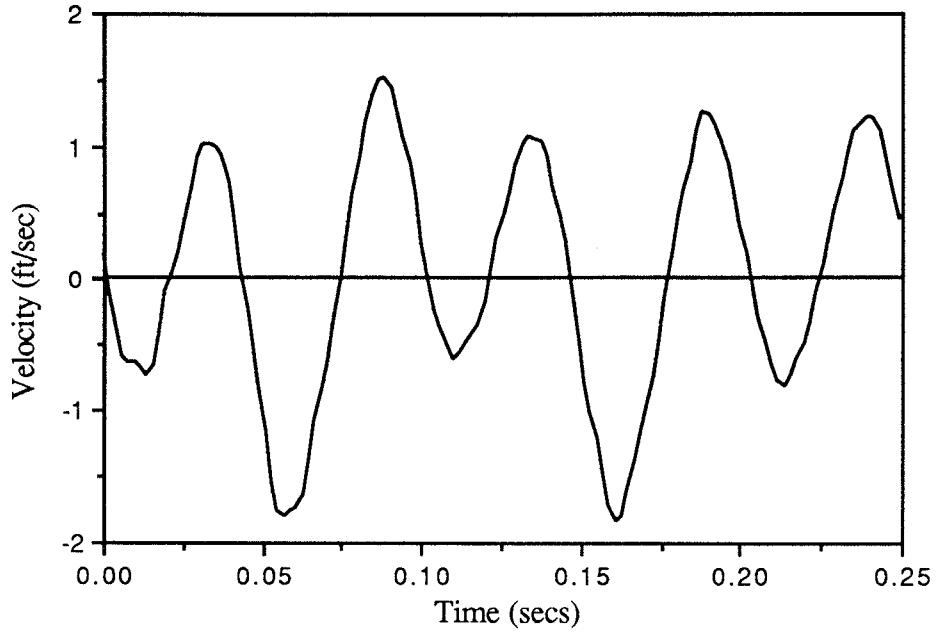


Fig. C3. Corrected Average Pile-Head Velocity vs Time at 86 ft Penetration Depth

DRIVING HISTORY OF PILE TP-1

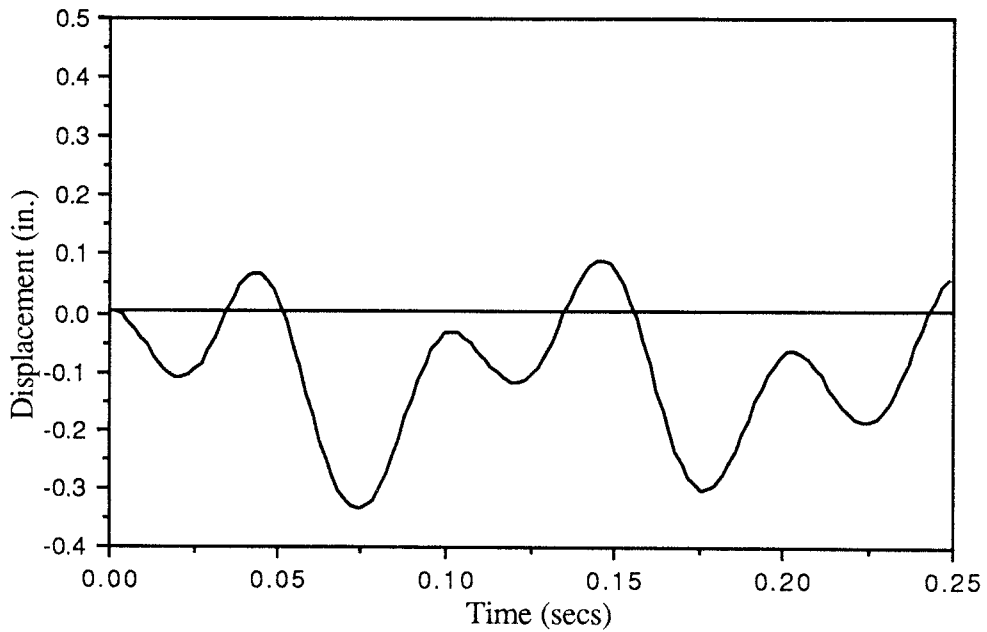


Fig. C4. Displacement vs Time at 86 ft Penetration Depth

DRIVING HISTORY OF PILE TP-4

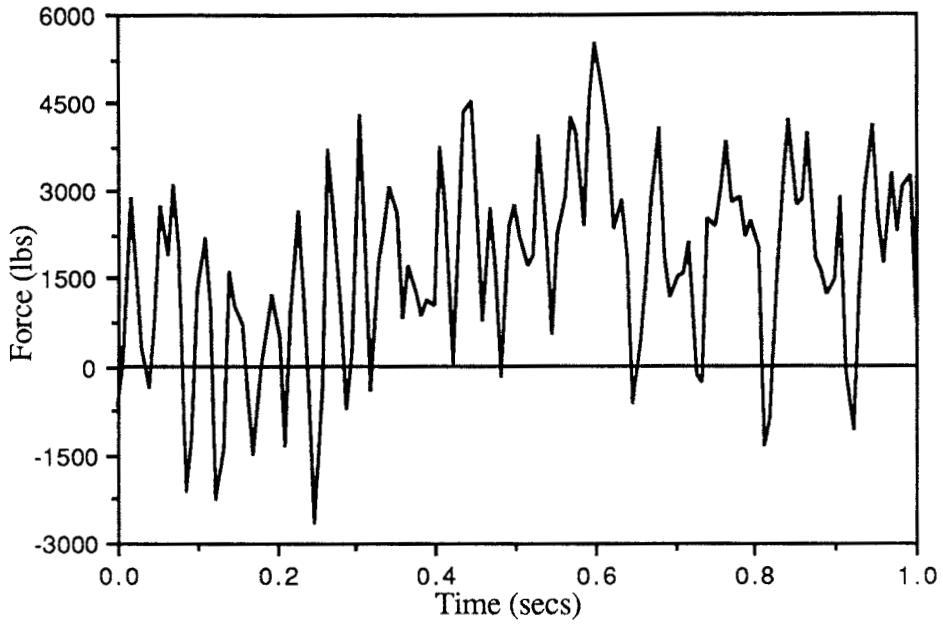


Fig. C5. Pile-Head Force vs Time at 50 ft Penetration Depth

DRIVING HISTORY OF PILE TP-4

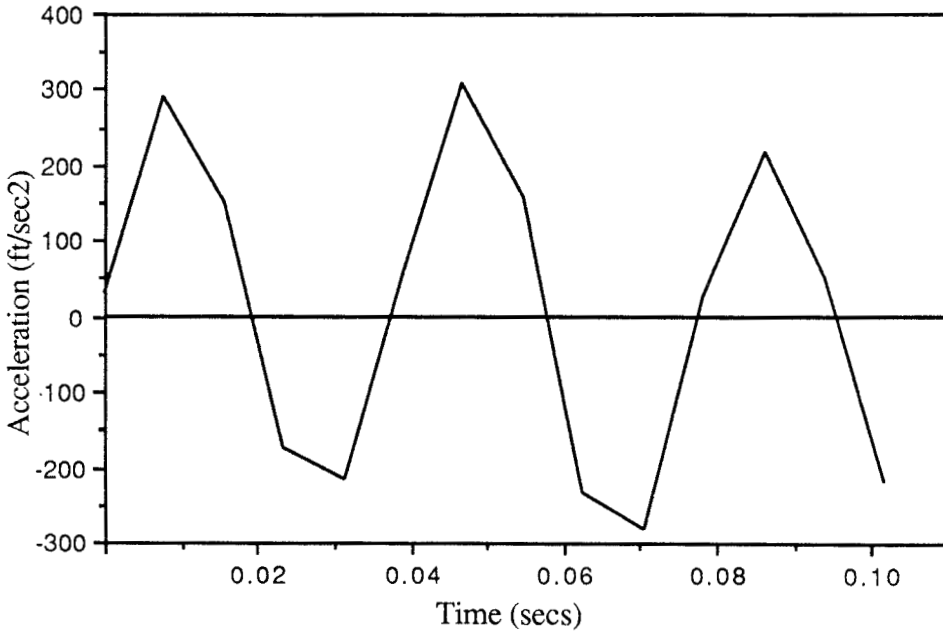


Fig. C6. Corrected Average Pile-Head Acceleration vs Time at 50 ft Penetration Depth

DRIVING HISTORY OF PILE TP-4

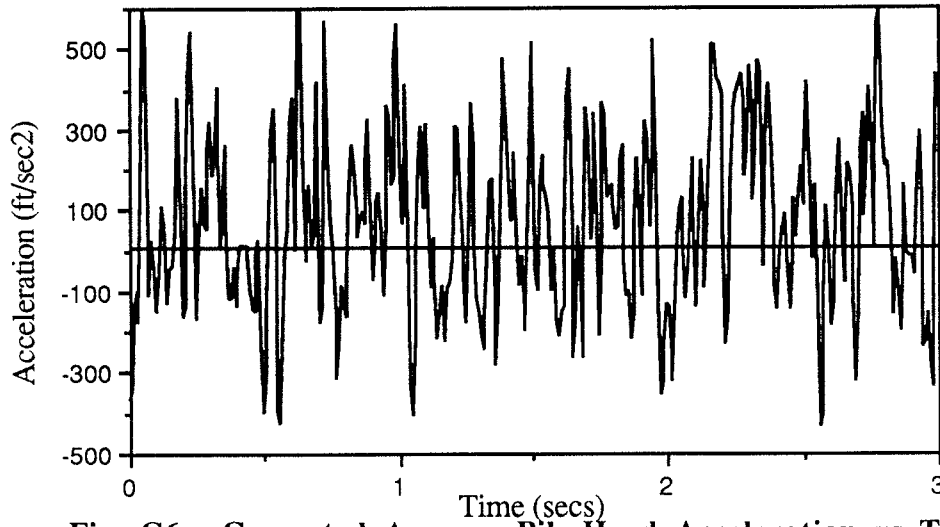


Fig. C6a. Corrected Average Pile-Head Acceleration vs Time at 50 ft Penetration Depth

DRIVING HISTORY OF PILE TP-4

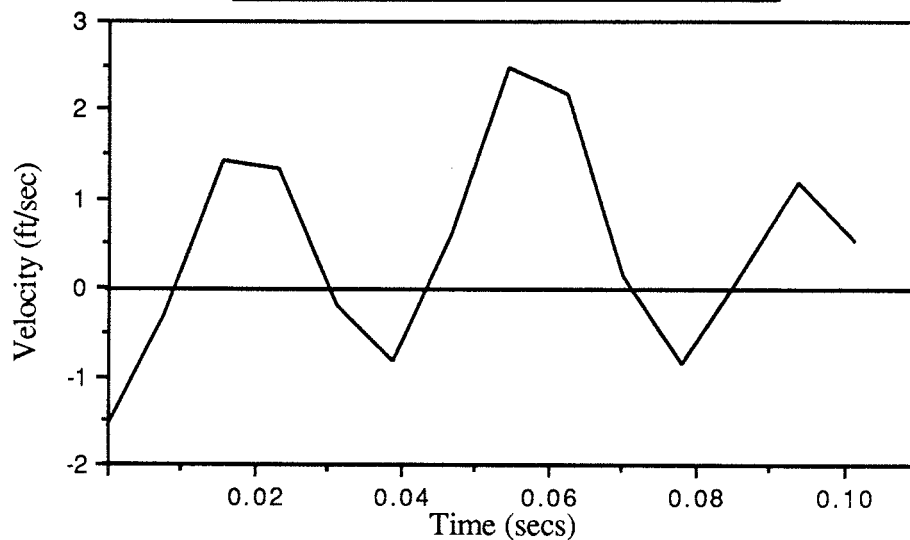


Fig. C7. Corrected Average Pile-Head Velocity vs Time at 50 ft Penetration Depth

DRIVING HISTORY OF PILE TP-4

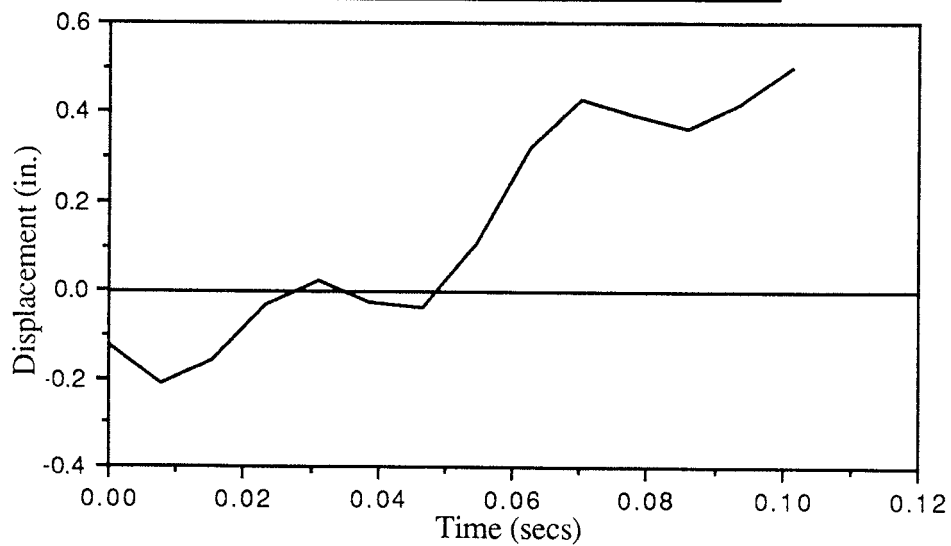


Fig. C8. Displacement vs Time at 50 ft Penetration Depth

DRIVING HISTORY OF PILE 559

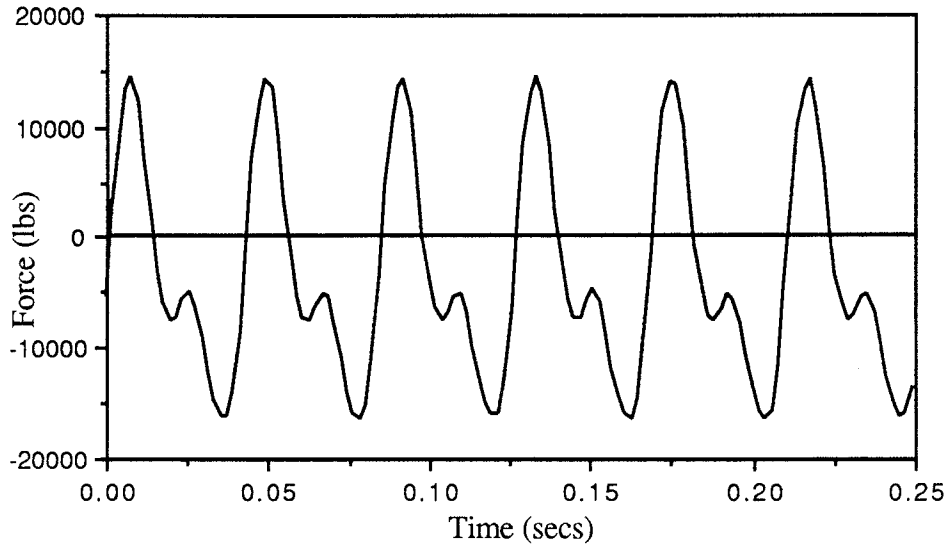


Fig.C9. Pile-Head Force vs Time at 82 ft Penetration Depth

DRIVING HISTORY OF PILE 559

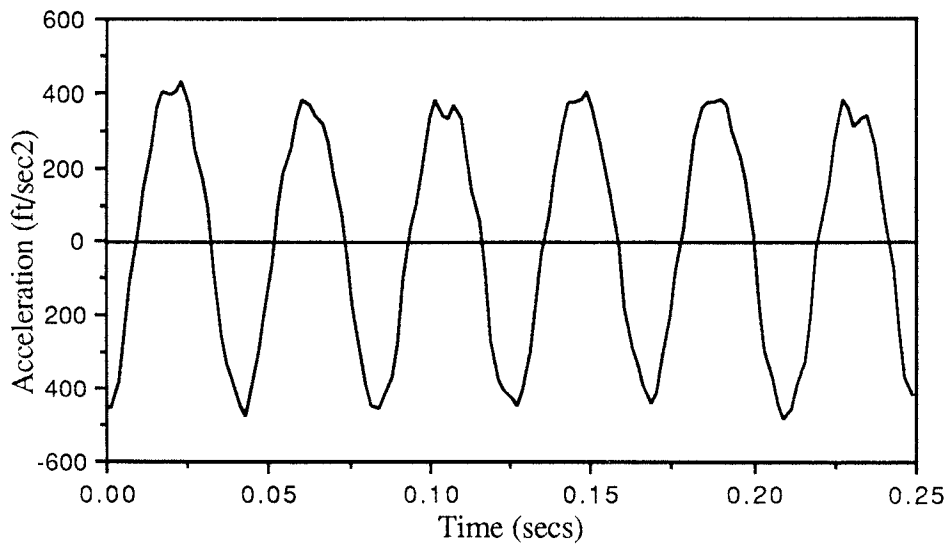


Fig. C10. Corrected Average Pile-Head Acceleration vs Time at 82 ft Penetration Depth

DRIVING HISTORY OF PILE 559

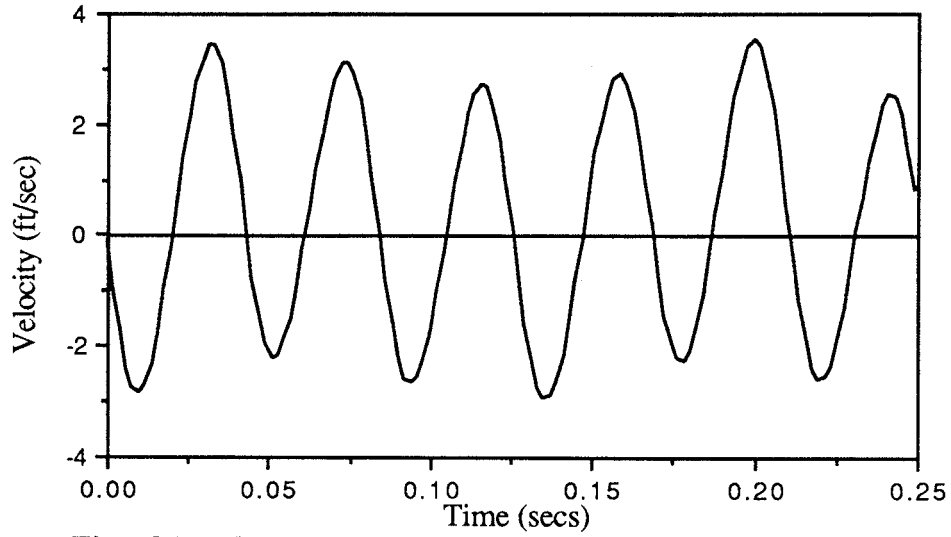


Fig. C11. Corrected Average Pile-Head Velocity vs Time at 82 ft Penetration Depth

DRIVING HISTORY OF PILE 559

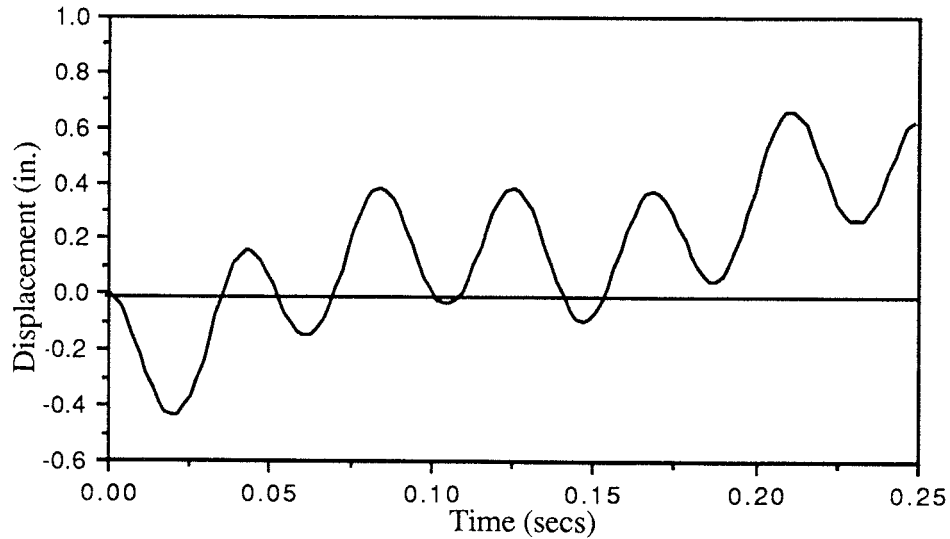


Fig. C12. Displacement vs Time at 82 ft Penetration Depth

DRIVING HISTORY OF PILE 619

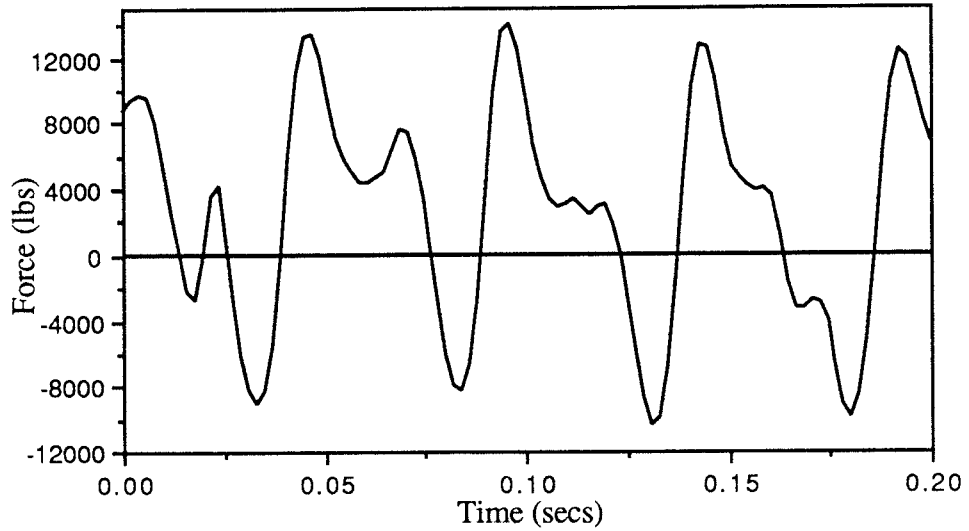


Fig. C13. Pile-Head Force vs Time at 72 ft Penetration Depth

DRIVING HISTORY OF PILE 619

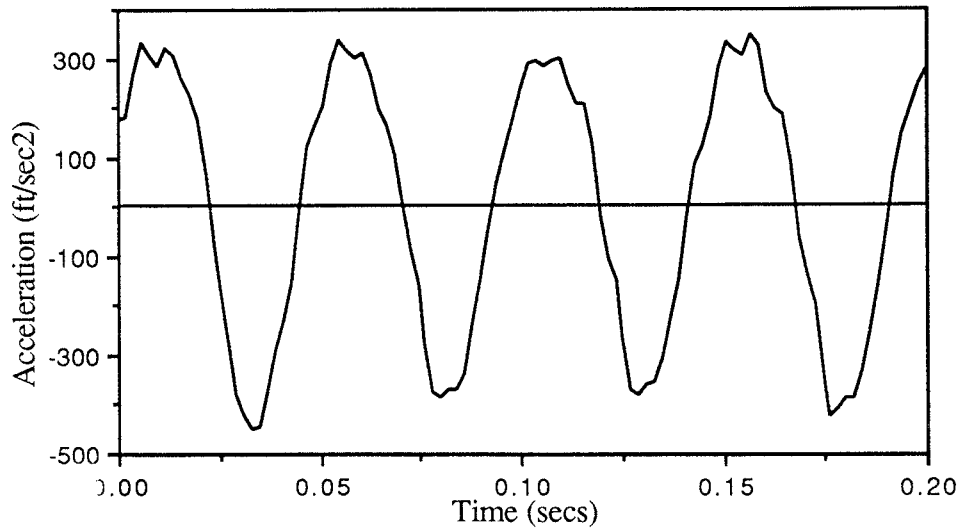


Fig. C14. Corrected Average Pile-Head Acceleration vs Time at 72 ft Penetration Depth

DRIVING HISTORY OF PILE 619

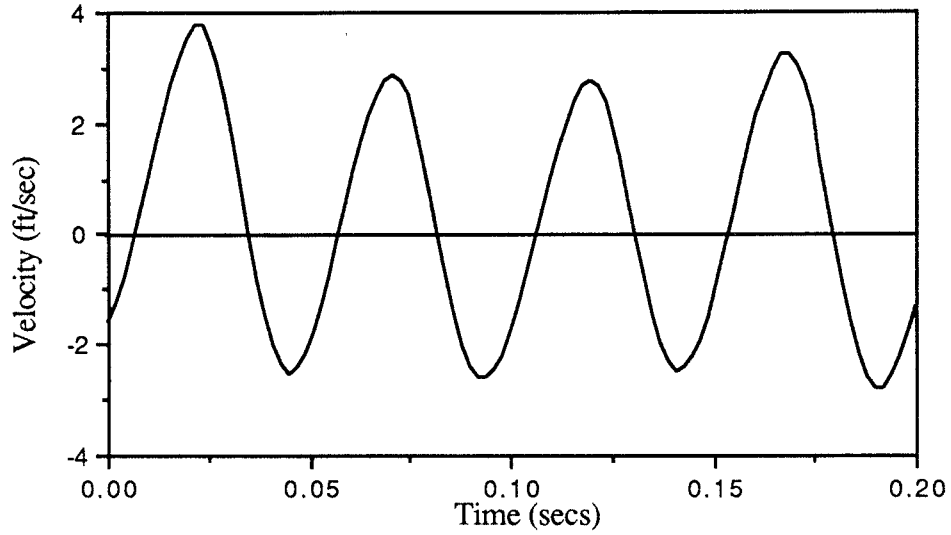


Fig. C15. Corrected Average Pile-Head Velocity vs Time at 72 ft Penetration Depth

DRIVING HISTORY OF PILE 619

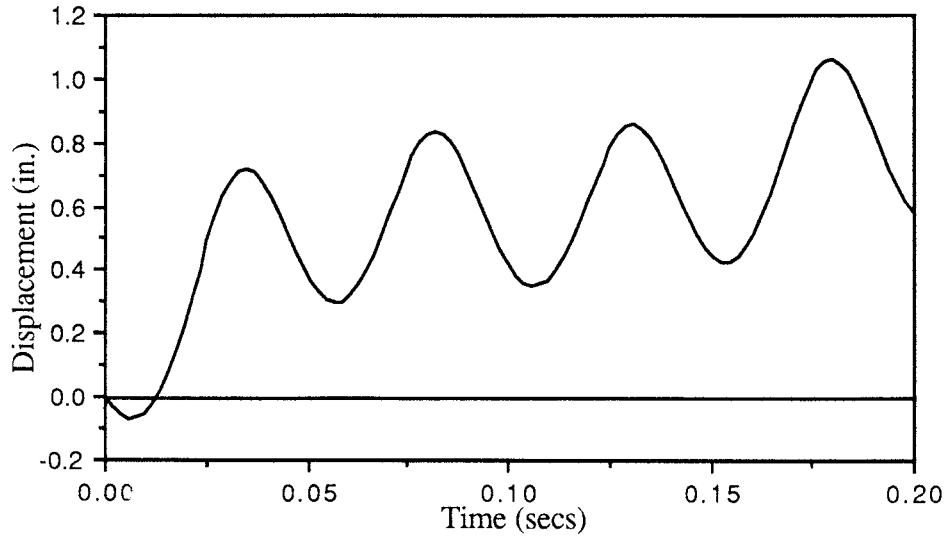


Fig. C16. Displacement vs Time at 72 ft Penetration Depth

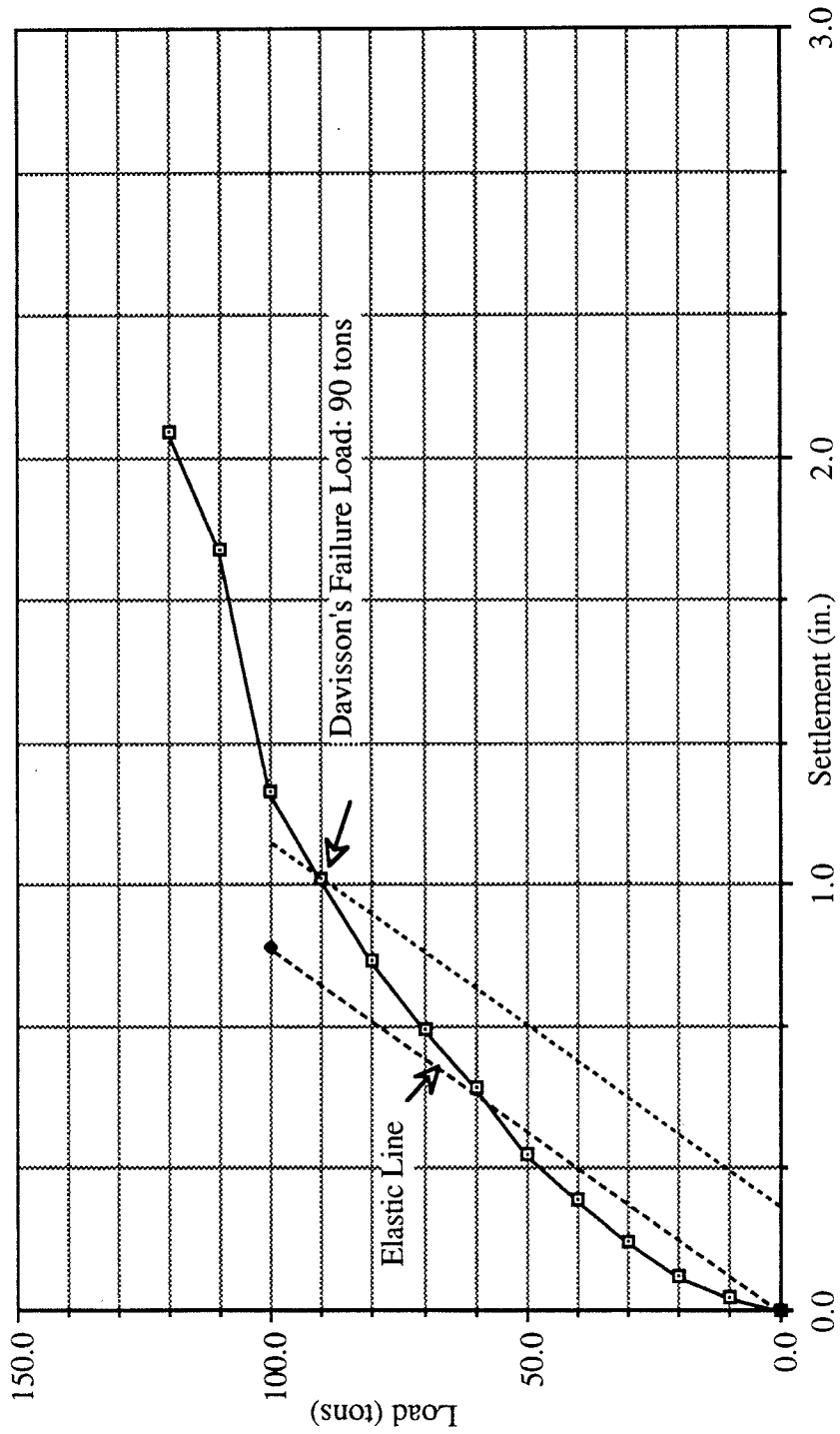


Fig. C17. Pile-Head Load vs Settlement Curve for TP-1

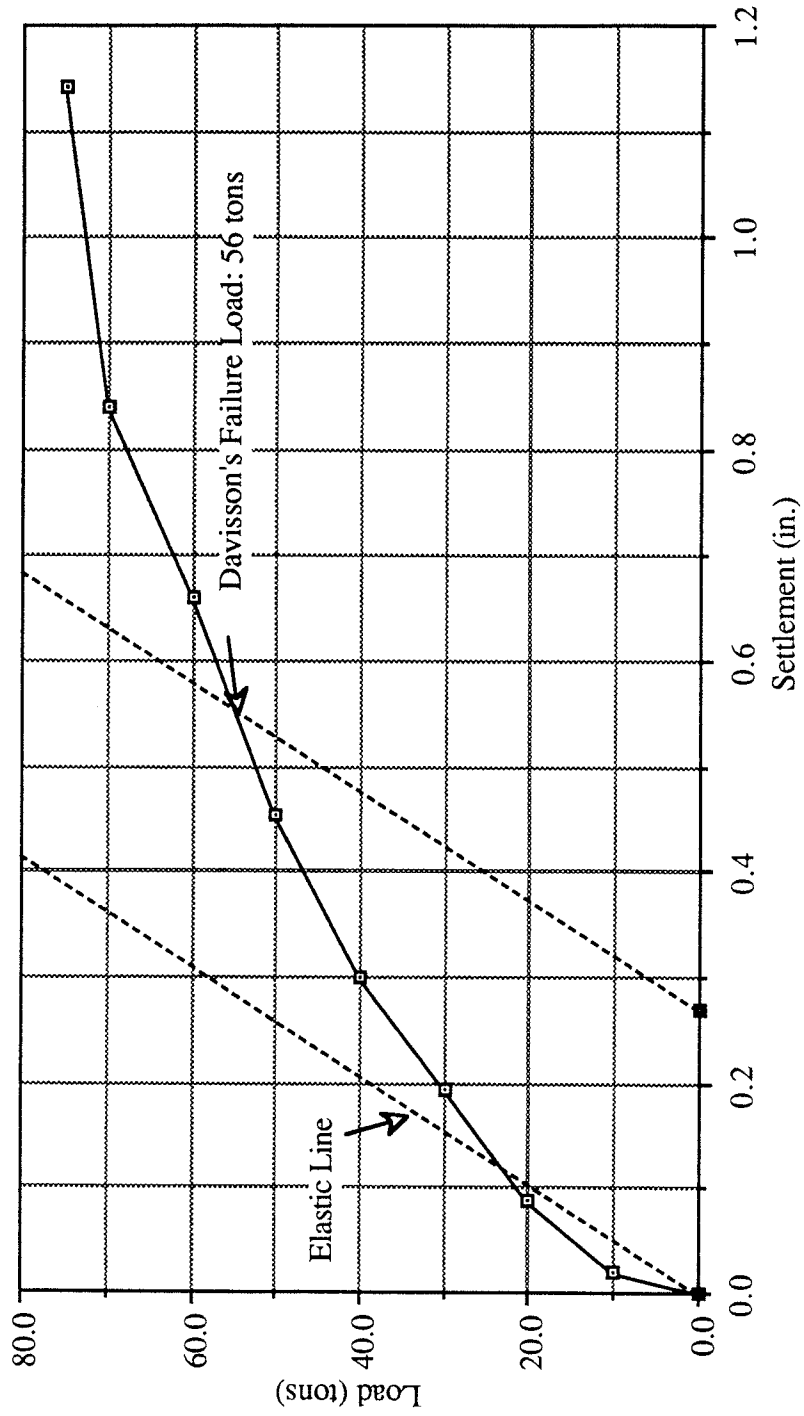


Fig. C18. Pile-Head Load vs Settlement Curve for TP-4

Table. C1. Rate of Penetration of Piles, Pioneer Freezer Site

Pile Penetration Below G.S (feet)	Pile TP-1 Elapsed Time (secondes)	Pile TP-4 Elapsed Time (secondes)	Pile 559 Elapsed Time (secondes)	Pile 619 Elapsed Time (secondes)
24	0			
25	4			
26	9			
27	18	0	0	
28	23	4	4	
29	25	7	9	
30	31	9	15	
31	35	11	20	
32	37	13	24	
33	39	14	35	
34	46	15	41	
35	50	16	49	
36	54	19	55	0
37	59	21	61	13
38	64	23	68	29
39	67	25	75	44
40	71	27	82	55
41	73	29	89	69
42	78	30	96	83
43	83	33	109	100
44	86	35	118	119
45	91	36	128	144
46	93	39	166	163
47	97	42	178	186
48	101	45	189	208
49	105	46	196	223
50	108	49	204	230
51	111	51	210	235
52	115	53	216	240
53	117	57	222	246
54	120	58	233	253
55	123	60	248	261
56	128	65	259	267
57	130	67	271	273
58	133	69	282	280
59	138	71	296	286
60	141	73	308	293
61	143	74	321	299
62	147	76	336	302
63	152	78	390	307
64	157	79	463	314
65	162	85	488	320
66	166	88	509	325
67	170	90	513	329
68	173	91	520	336

Table. C1. Continued

69	175	92	528	346
70	179	93	535	406
71	182	94	543	524
72	185	96	568	630
73	188	98	613	
74	193	103	650	
75	198	104	671	
76	230	118	687	
77	233	127	699	
78	235	154	705	
79	238	206	708	
80	240	270	716	
81	242		720	
82	244		723	
83	246			
84	301			
85	429			
86	478			

APPENDIX D

APPENDIX D

Laboratory Test Data

This appendix provides typical data from the laboratory tests, which were designated 2A and 7C.

General Conditions for Test 2A

Soil Parameters: San Jacinto River Sand (saturated)
Relative Density 65%
Effective Confining Pressure 10 psi
Overburden Pressure 10 psi

Vibrator Parameters: Unbalanced Moment 50 in-lb.
Bias Weight 1620 lb. + 380 lb.

Pile Type: 4" Diameter Closed Ended Steel Pipe Pile

General Conditions for Test 7C

Soil Parameters: San Jacinto River Sand (saturated)
Relative Density 65%
Effective Confining Pressure 10 psi
Overburden Pressure 10 psi

Vibrator Parameters: Unbalanced Moment 50 in-lb.
No Bias Weight

Pile Type: 3 in. Steel H Pile

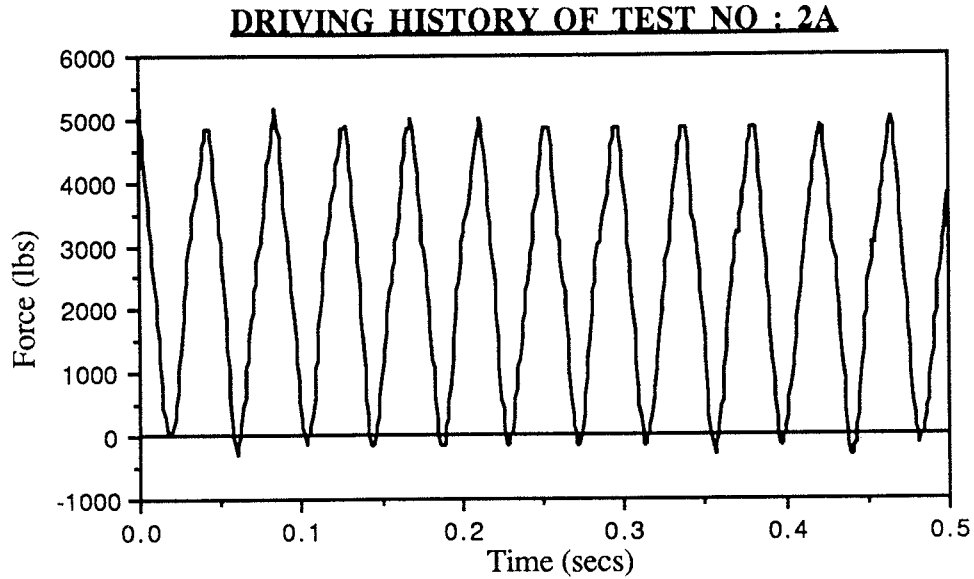


Fig. D1. Pile-Head Force vs Time at 75" Penetration Depth

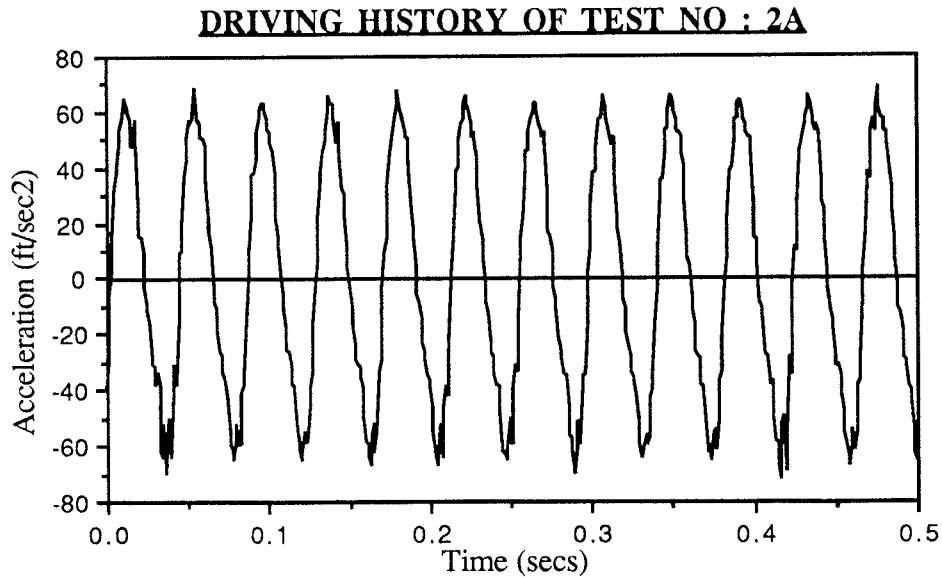


Fig. D2. Corrected Average Pile-Head Acceleration vs Time at 75" Penetration Depth

DRIVING HISTORY OF TEST NO : 2A

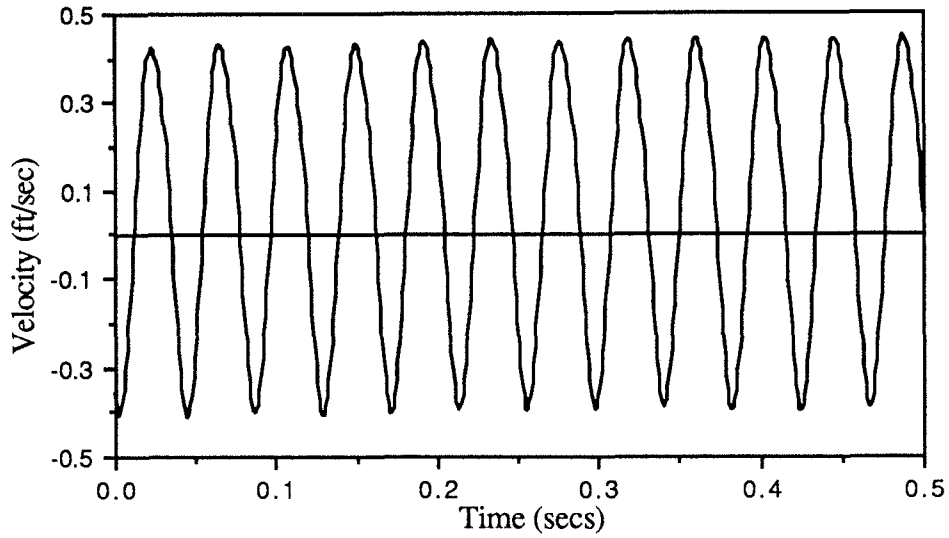


Fig. D3. Corrected Average Pile-Head Velocity vs Time at 75" Penetration Depth

DRIVING HISTORY OF TEST NO : 2A

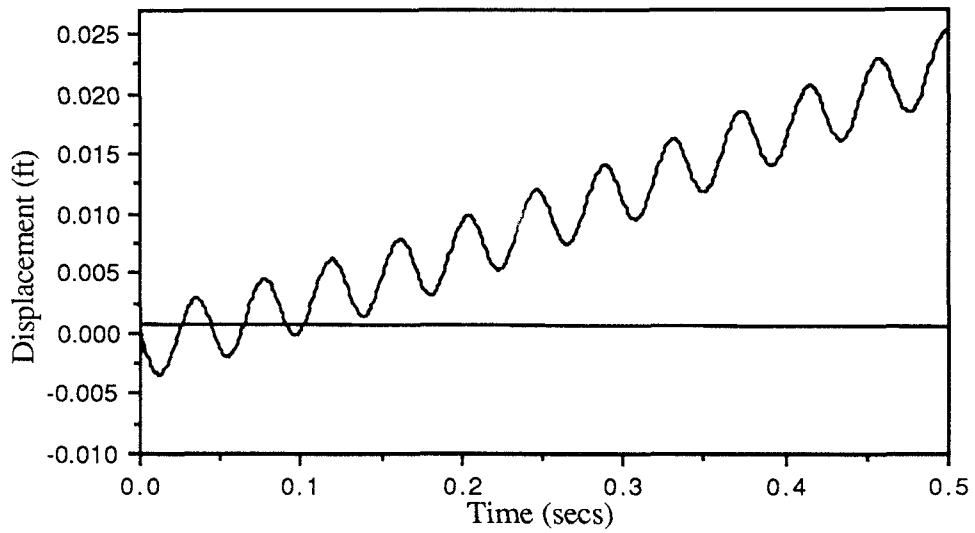


Fig. D4. Displacement vs Time at 75" Penetration Depth

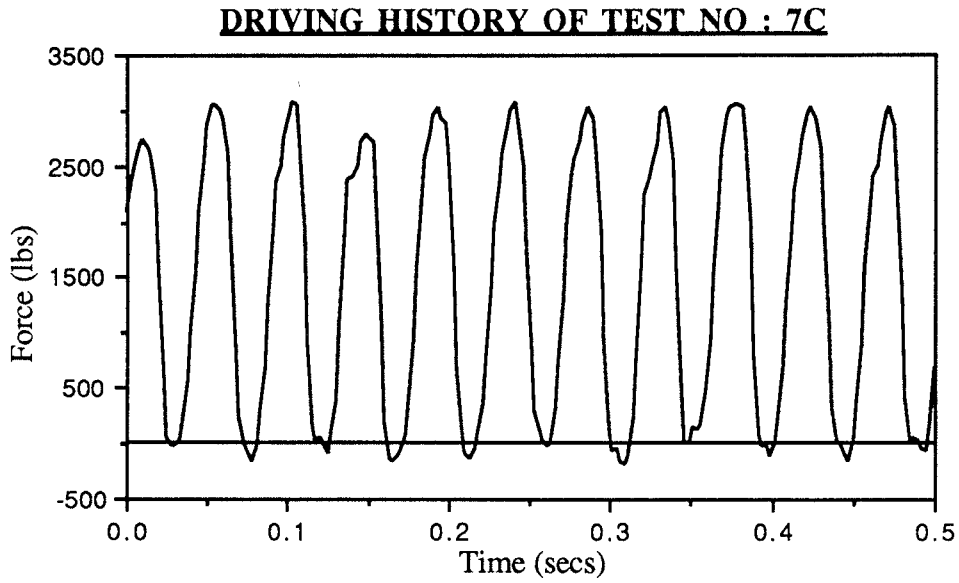


Fig. D5. Pile-Head Force vs Time at 75" Penetration Depth

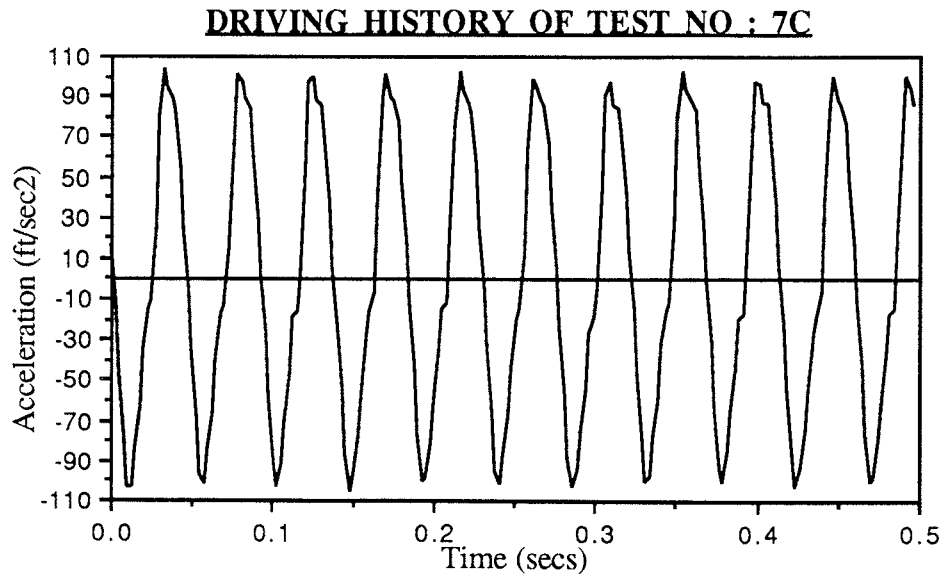


Fig. D6. Corrected Average Pile-Head Acceleration vs Time at 75" Penetration Depth

DRIVING HISTORY OF TEST NO : 7C

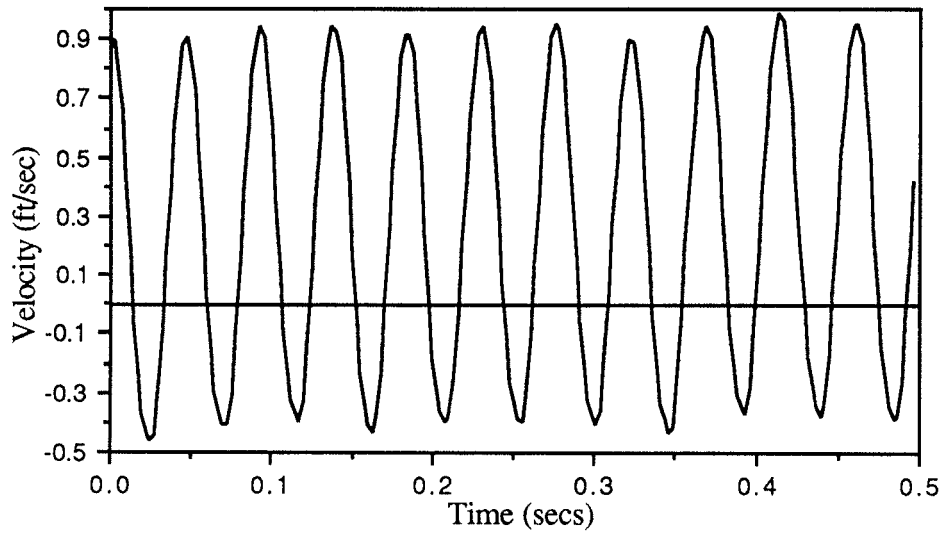


Fig. D7. Corrected Average Pile-Head Velocity vs Time at 75" Penetration Depth

DRIVING HISTORY OF TEST NO : 7C

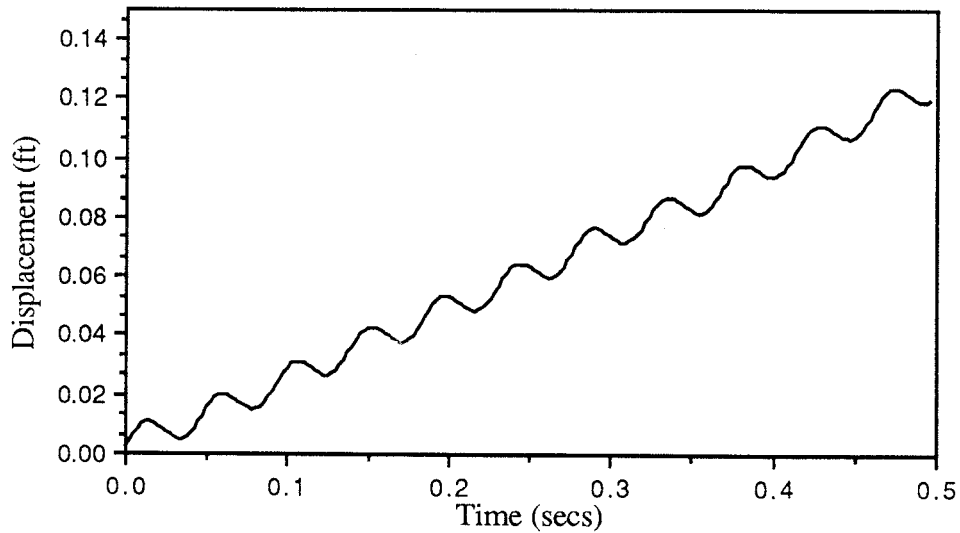


Fig. D8. Displacement vs Time at 75" Penetration Depth

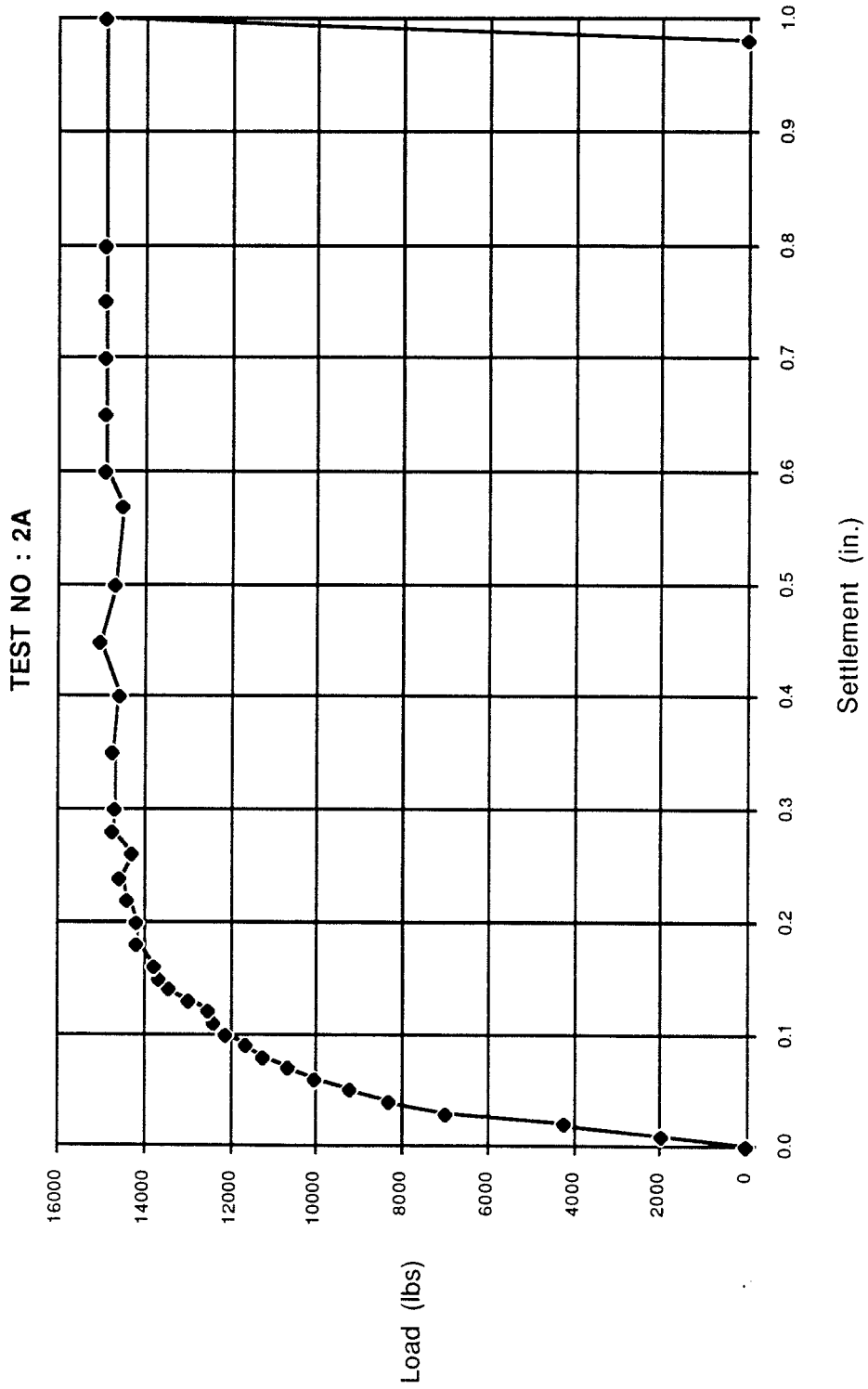


Fig. D9. Pile-Head Load vs Settlement Curve

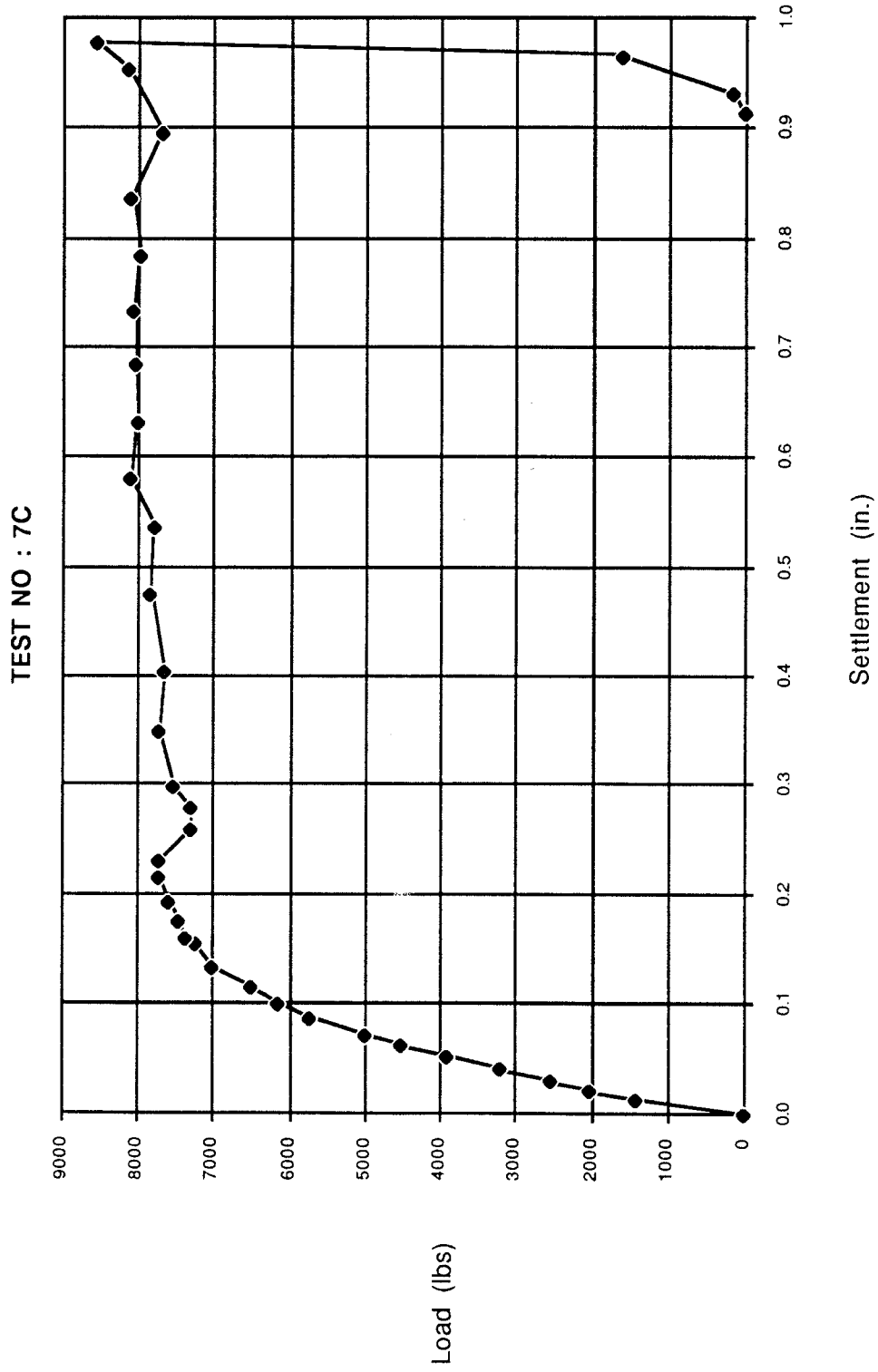


Fig. D10. Pile-Head Load vs Settlement Curve

APPENDIX E

Results of Parametric Study Conducted Upon Pile 2A

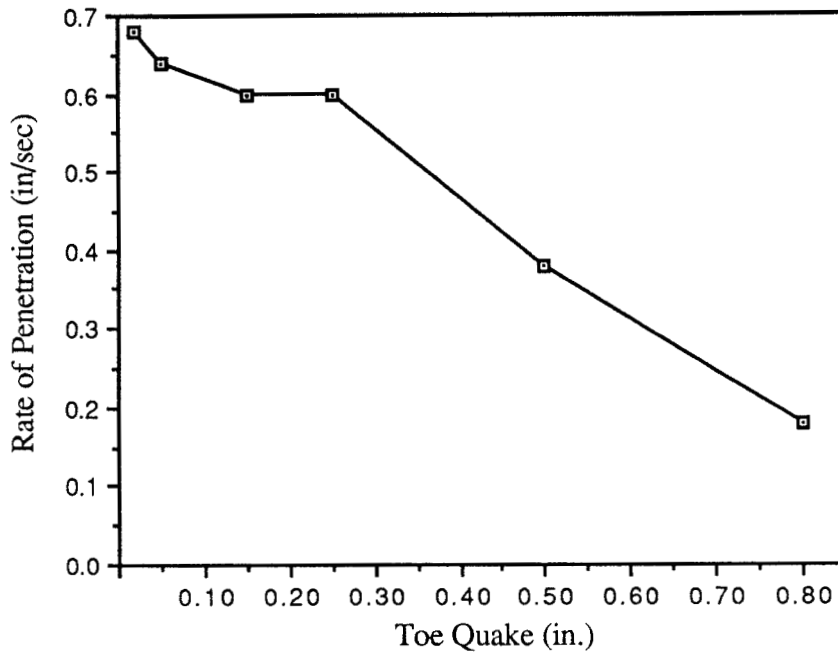


Fig. E1. Penetration Rate vs Toe Quake for test 2A

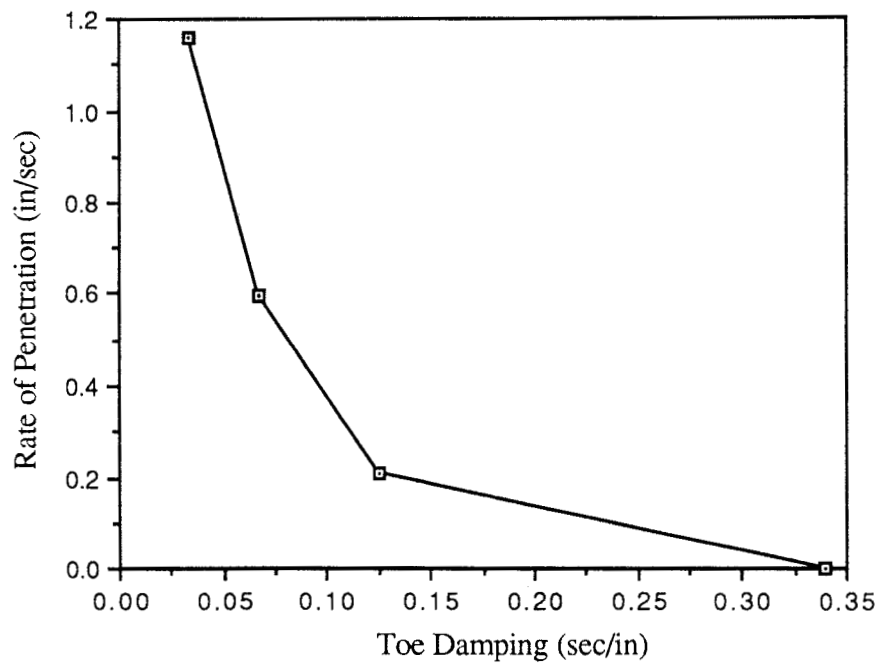


Fig. E2. Penetration Rate vs Toe Damping for test 2A

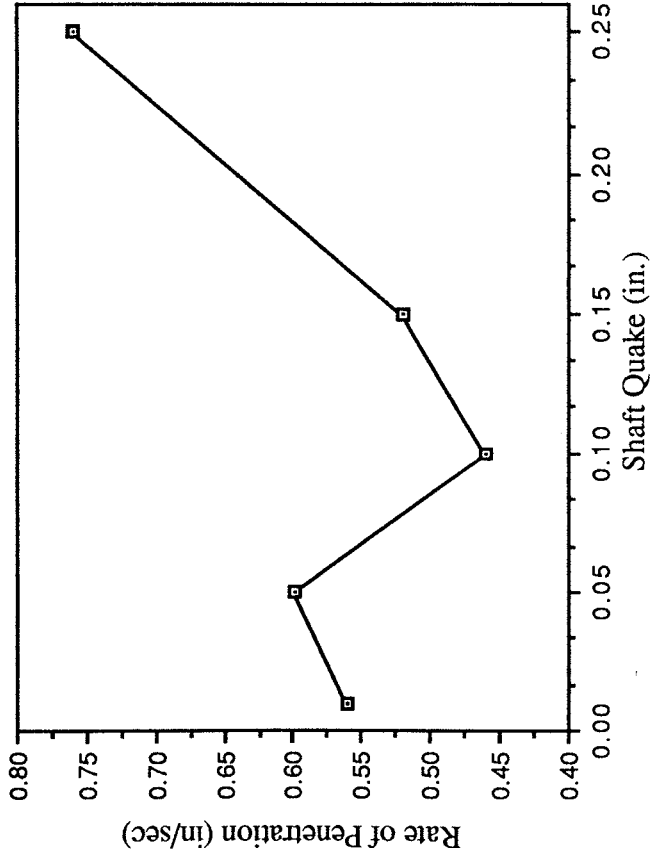


Fig. E3. Penetration Rate vs Shaft Quake for Test 2A

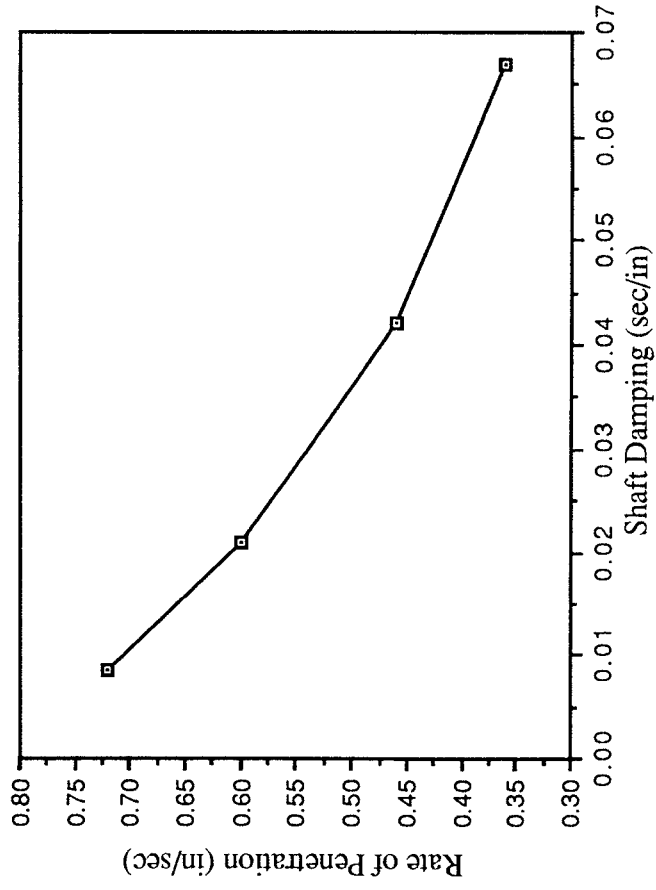


Fig. E4. Penetration Rate vs Shaft Damping for Test 2A

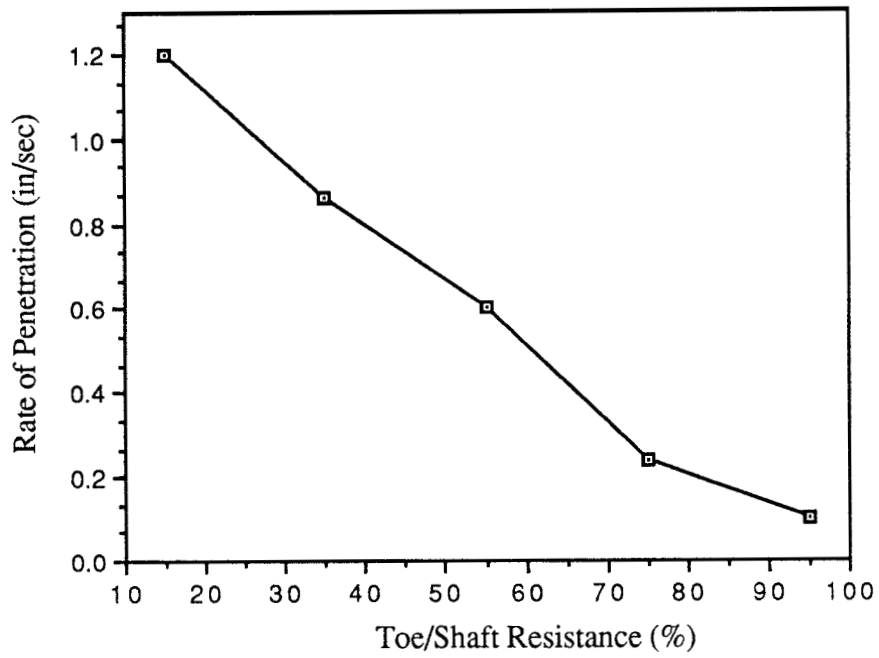


Fig. E5. Penetration Rate vs Toe/Shaft Resistance for Test 2A

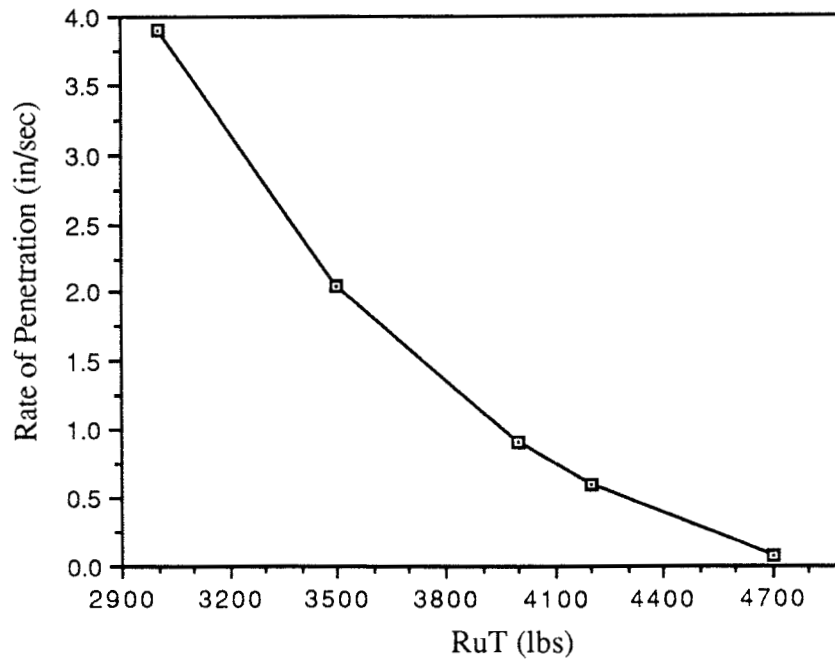


Fig. E6. Penetration Rate vs RuT for Test 2A

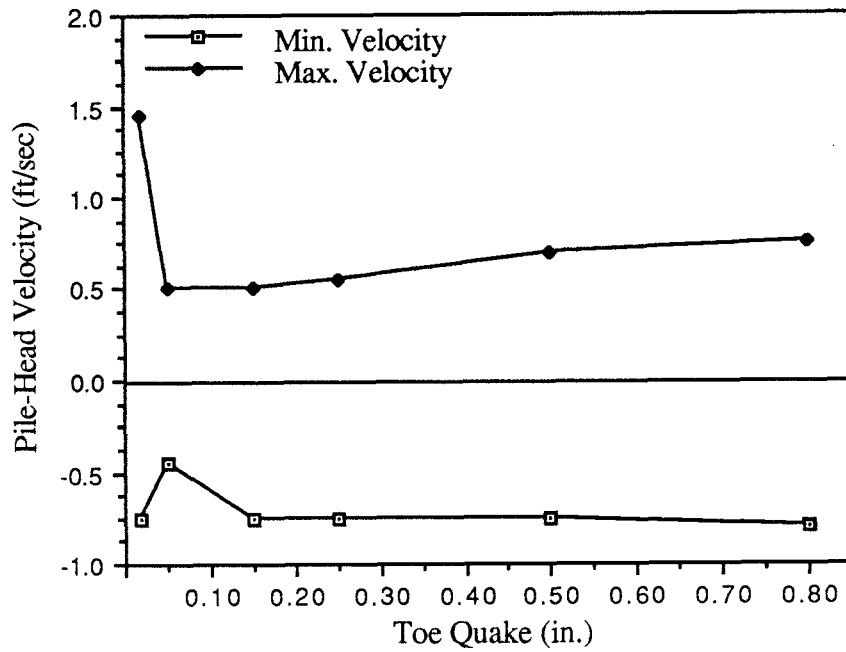


FIG. E7. Peak to Peak Velocity vs Toe Quake for Test 2A

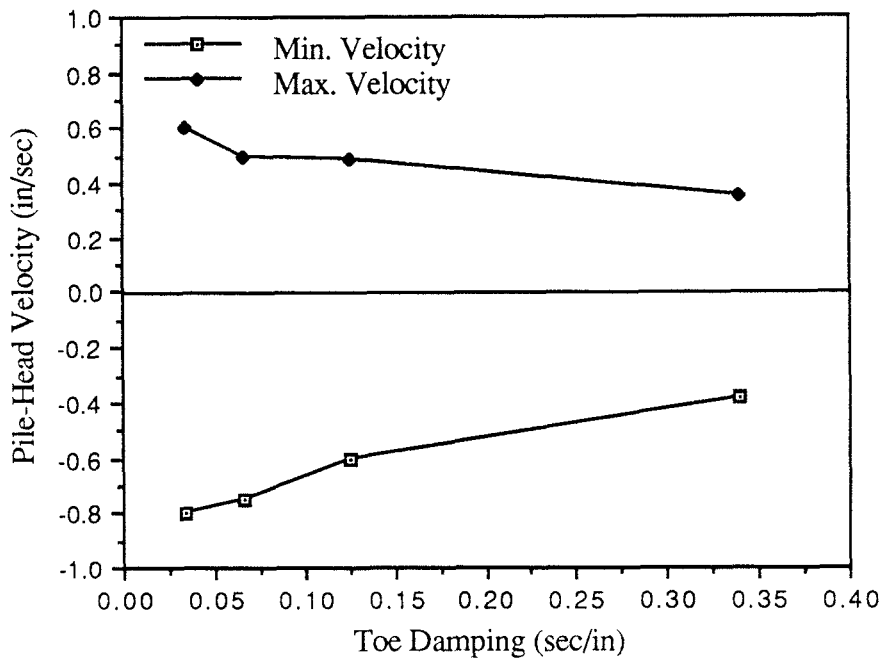


Fig. E8. Peak to Peak Velocity vs Toe Damping for Test 2A

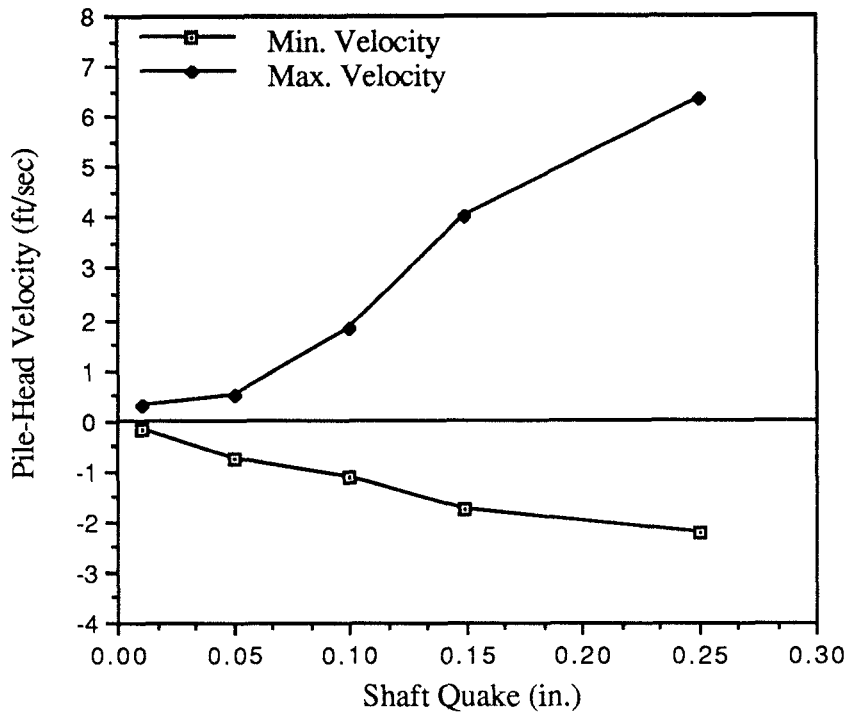


Fig. E9. Peak to Peak Velocity vs Shaft Quake for Test 2A

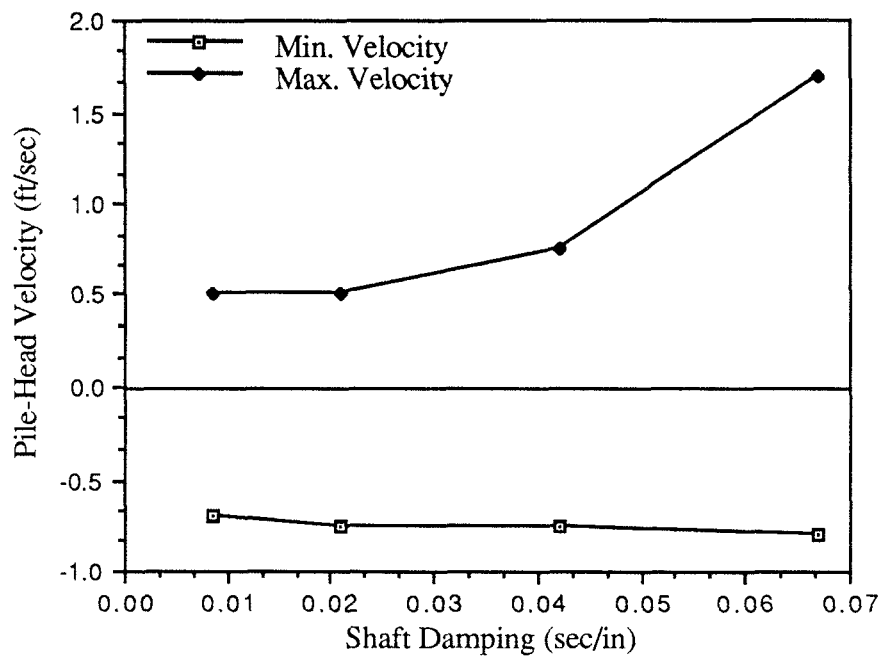


Fig. E10. Peak to Peak Velocity vs Shaft Damping for Test 2A

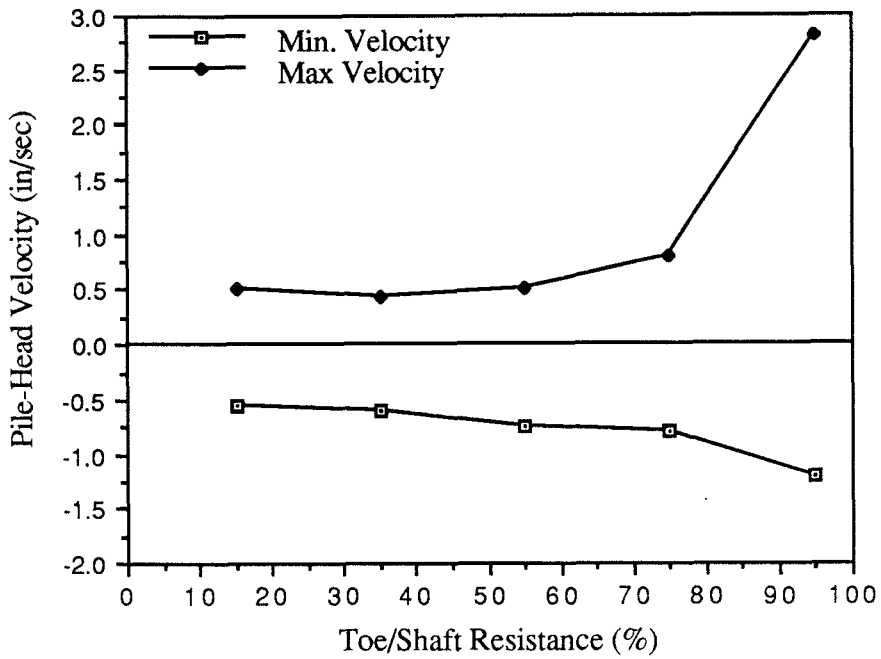


Fig. E11. Peak to Peak Velocity vs Toe/Shaft Resistance for Test 2A

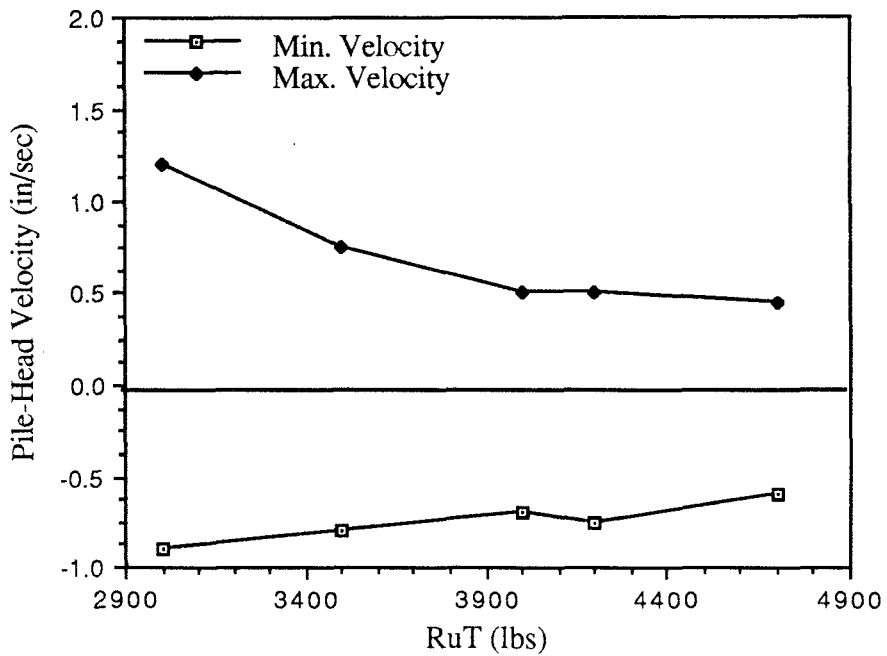


Fig. E12. Peak to Peak Velocity vs RuT for Test 2A